European Journal of Medicinal Chemistry 222 (2021) 113542

Contents lists available at ScienceDirect

European Journal of Medicinal Chemistry

journal homepage: http://www.elsevier.com/locate/ejmech

Design, synthesis, and biological evaluation of novel sulindac derivatives as partial agonists of PPARγ with potential anti-diabetic efficacy

Fengyu Huang [a, 1], Zhiping Zeng [a, b, 1], Weidong Zhang [a], Zhiqiang Yan [a], Jiayun Chen [a], Liangfa Yu [a], Qian Yang [a], Yihuan Li [a], Hongyu Yu [a], Junjie Chen [a], Caisheng Wu [a], Xiao-kun Zhang [a, b], Ying Su [c, **], Hu Zhou [a, b, *]

[a] School of Pharmaceutical Sciences, Fujian Provincial Key Laboratory of Innovative Drug Target Research, Xiamen University, Xiamen, Fujian, 361102, China
[b] High Throughput Drug Screening Platform, Xiamen University, Xiamen, Fujian, 361102, China
[c] NucMito Pharmaceuticals, Xiamen, Fujian, 361101, China

ARTICLE INFO

Article history:
Received 8 February 2021
Received in revised form
30 April 2021
Accepted 7 May 2021
Available online 24 May 2021

Keywords:
Sulindac derivatives
PPARγ
Partial agonists
Diabetes
Insulin resistance
Meta-substitution

ABSTRACT

Peroxisome proliferator-activated receptor gamma (PPARγ) is a valuable drug target for diabetic treatment and ligands of PPARγ have shown potent anti-diabetic efficacy. However, to overcome the severe side effects of current PPARγ-targeted drugs, novel PPARγ ligands need to be developed. Sulindac, an identified ligand of PPARγ, is widely used in clinic as a non-steroidal anti-inflammatory drug. To explore its potential application for diabetes, we designed and synthesized a series of sulindac derivatives to investigate their structure-activity relationship as PPARγ ligand and potential anti-diabetic effect. We found that *meta*-substitution in sulindac's benzylidene moiety was beneficial to PPARγ binding and transactivation. *Z* rather than *E* configuration of the benzylidene double bond endowed derivatives with the selectivity of PPARγ activation. The indene fluorine is essential for binding and regulating PPARγ. Compared with rosiglitazone, compound **6b** with benzyloxyl *meta*-substitution and *Z* benzylidene double bond weakly induced adipogenesis and PPARγ-targeted gene expression. However, **6b** potently improved glucose tolerance in a diabetic mice model. Unlike rosiglitazone, **6b** was devoid of apparent toxicity to osteoblastic formation. Thus, we provided some useful guidelines for PPARγ-based optimization of sulindac and an anti-diabetic lead compound with less side effects.

1. Introduction

Peroxisome proliferator-activated receptor gamma (PPARγ) belonging to nuclear receptor superfamily is a major regulator in adipocyte differentiation, lipid metabolism, glucose homeostasis and insulin sensitivity [1–3]. The physiopathological activities of PPARγ are tightly controlled by its endogenous and exogenous ligands including 15-deoxy-delta 12,14-prostaglandin J_2, eicosapentaenoic acid, 9-HODE, and 13-HODE [4–8], while its pharmacological modulation by ligands has been applied to the treatment of diabetes [9]. Actos (pioglitazone) and Avandia (rosiglitazone), the two potent agonists of PPARγ, effectively increase insulin sensitization and improve glycemic control in patients with type 2 diabetes [10–12]. However, strong PPARγ-activating drugs were once withdrawn from the market or had restricted prescription due to their severe adverse effects such as weight gain, edema, liver injury and heart failure [13,14]. In addition, PPARγ and its potent ligands also negatively regulate osteoblastogenesis, increasing the risk of osteoporosis. Thus, novel PPARγ-targeting drugs with less above side effects should be devised for diabetes treatment [15].

Repositioning of clinical drugs is a promising strategy for drug development [16–18]. Sulindac, a non-steroidal anti-inflammatory drug (NSAID), binds to PPARγ and regulates PPARγ activity, as well as exerts PPARγ-dependent physiological activities [19–21]. However, sulindac has its well-known adverse effects from long-term

* Corresponding author. School of Pharmaceutical Sciences, Xiamen University, Xiamen, Fujian, 361102, China.
**Corresponding author. NucMito Pharmaceuticals, Xiamen, Fujian, 361101, China.
E-mail addresses: ying.su@nucmito.com (Y. Su), huzhou@xmu.edu.cn (H. Zhou).
[1] These authors have contributed equally to this work.

https://doi.org/10.1016/j.ejmech.2021.113542
0223-5234/

clinical application, including potential gastrointestinal and cardiovascular side effects mostly owning to its potent inhibition of cyclooxygenases (COX-1 and COX-2) [22]. We and others have shown that the methythiol group of sulindac sulfide metabolized from methyl sulfoxide of sulindac is essential for COX inhibition [23,24]. However, the PPARγ-dependent structure-activity relationship (SAR) of sulindac derivatives needs to be comprehensively defined.

Felts et al. has reported that the optimized derivative of sulindac (compound **24**, Scheme 1) binds to PPARγ and regulates PPARγ activities with slightly improved EC_{50} value compared with that of the hit *Z*-sulindac sulfide [25]. A disadvantage of compound **24** is its less selectivity in PPARγ regulation because it activates both PPARα and PPARγ. Furthermore, the sulindac derivatives reported in Felts's work are of the *E* benzylidene double bond, while the geometric isomerism of the benzylidene double bond is *Z* in sulindac and sulindac sulfide (Scheme 1). Also, all the derivatives they reported are *E*-2′-des-methyl (removal of the indenyl methyl group). These altered geometric isomerism may lead to distinct metabolic modes and side effects between sulindac and these derivatives. In addition, according to the crystal structure of sulindac-PPARγ complex, the ligand binding pocket (LBP) of PPARγ is large enough to adopt two sulindac molecule [26], which seems to complicate the design of its further optimization.

In this work, we designed and synthesized a series of sulindac derivatives with the core scaffold unchanged and the methyl sulfoxide group replaced, and evaluated their PPARγ-based SAR and anti-diabetic activity.

2. Results and discussion

2.1. Chemistry

Synthesis method of indenone (**Rec1** and **Rec2**, Scheme 2) from starting materials (various benzaldehydes) by Perkin reaction, hydrogenation and Friedel-Crafts reaction was described in our previous papers (see Scheme 2), and the characterization of compounds **1**, **2**, **4a** and **10** were also shown in our published papers [23,27,28]. The general synthesis process for intermediates **Rec1** and **Rec2** is shown in method section. The methyl group (purple) in indene gives predominantly *Z*-isomers. Our target molecules were produced by the condensation reaction between indene and different substituted aromatic aldehydes using standard method described also in our previous papers (see Scheme 2).

2.2. SAR study of sulindac derivatives

We found that sulindac only slightly activated Gal4/DBD-PPARγ/LBD chimera transactivation in our mammalian-one-hybrid assay (EC_{50}: 22.65 ± 2.94 μM, max fold induction: 1.34 ± 0.10) (Table 1, compound **1**). In order to remove its COX inhibition activity, the methyl sulfoxide was substituted to hydrogen to obtain compound **2**. Interestingly, **2** had higher potency (EC_{50}: 2.78 ± 0.70 μM) and efficacy (max fold induction: 3.62 ± 1.47) than sulindac for inducing PPARγ transactivation (Table 1 and Supplementary Fig. 1). Consistently, **2** had higher PPARγ binding affinity (K_D = 7.94 ± 1.83 μM) than sulindac (K_D > 100 μM) according to our fluorescence titration

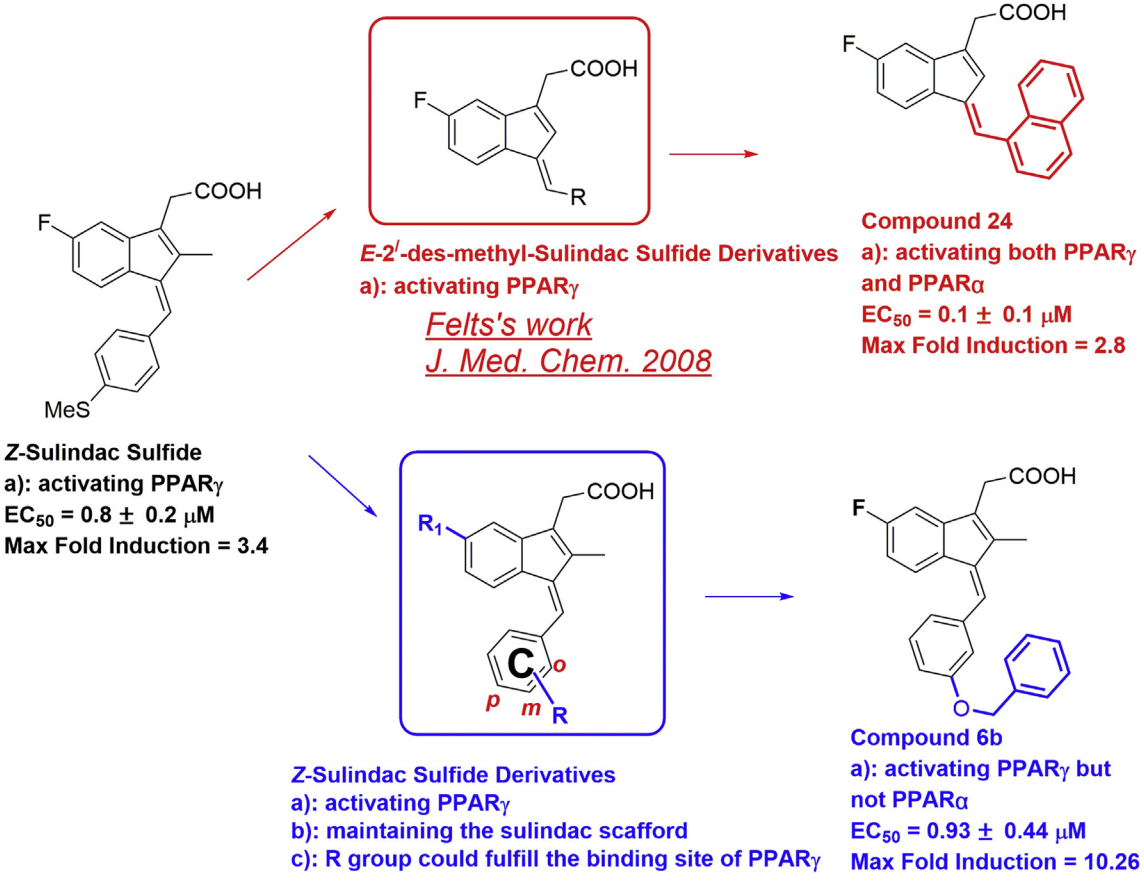

Scheme 1. Design strategy for novel sulindac analogues targeting to PPARγ.

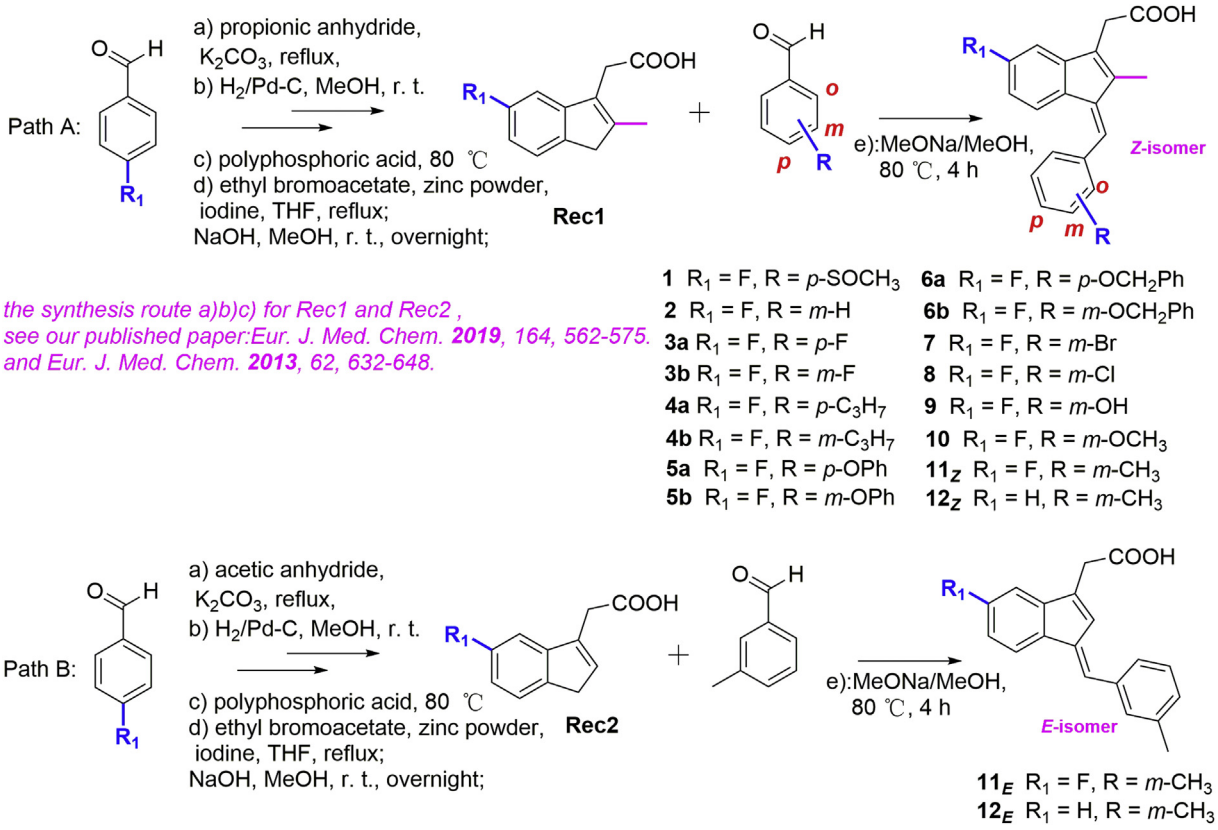

Scheme 2. General synthesis method for the sulindac analogues **1** - **12$_E$**. a): Propionic or acetic anhydride, K_2CO_3, reflux. b): H_2/Pd-C, MeOH, r. t. c): Polyphosphoric acid (PPA), 80 °C d): Reformatsky reaction, ethyl bromoacetate, zinc powder, iodine, THF, reflux; NaOH, MeOH, r. t., overnight; e): MeONa/MeOH, 80 °C, 4 h.

Table 1
The study of compounds on PPARγ binding and transcriptional activation.

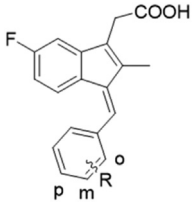
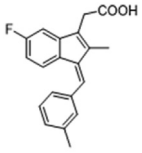
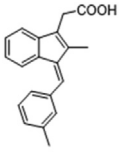
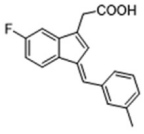
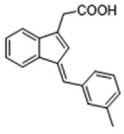

11_Z **12_Z** **11_E** **12_E**

Compound ID	Indene Fluorine	R group position	R Group Type	*E,Z* Configuration	EC_{50} (μM)[a] (PPARγ TA)	Max Fold Induction[b] (PPARγ TA)	K_D (μM)[c] (PPARγ Binding)
1	+	*p*	-$SOCH_3$	*Z*	22.65±2.94	1.34±0.10	>100
2	+	*m*	-H	*Z*	2.78 ± 0.70	3.62 ± 1.47	7.94 ± 1.83
3a	+	*p*	-F	*Z*	11.66 ± 1.95	3.18 ± 0.47	6.67 ± 0.65
3b	+	*m*	-F	*Z*	1.84 ± 0.30	7.53 ± 2.20	1.80 ± 0.41
4a	+	*p*	-C_3H_7	*Z*	>50	<1.10	>100
4b	+	*m*	-C_3H_7	*Z*	6.41 ± 0.93	4.39 ± 0.98	2.47 ± 0.58
5a	+	*p*	-OPh	*Z*	>50	<1.10	>100
5b	+	*m*	-OPh	*Z*	1.178 ± 0.27	9.03 ± 0.40	1.73 ± 0.65
6a	+	*p*	-OCH_2Ph	*Z*	>50	<1.10	>100
6b	+	*m*	-OCH_2Ph	*Z*	0.93 ± 0.44	10.26 ± 0.94	0.96 ± 0.35
7	+	*m*	-Br	*Z*	4.61 ± 1.48	6.80 ± 0.63	1.70 ± 1.71
8	+	*m*	-Cl	*Z*	1.74 ± 0.38	6.85 ± 2.66	1.22 ± 0.59
9	+	*m*	-OH	*Z*	6.29 ± 2.65	5.37 ± 0.21	5.52 ± 1.16
10	+	*m*	-OCH_3	*Z*	5.30 ± 1.28	4.65 ± 0.45	2.46 ± 1.20
11_Z	+	*m*	-CH_3	*Z*	12.02 ± 0.64	10.8 ± 0.92	4.00 ± 1.48
11_E	+	*m*	-CH_3	*E*	5.25 ± 2.00	6.59 ± 2.61	21.57 ± 2.24
12_Z	-	*m*	-CH_3	*Z*	>50	3.39 ± 1.59	>100
12_E	-	*m*	-CH_3	*E*	>50	2.57 ± 0.65	>100

[a] The potency of the compounds on activation of PPARγ were measured by mammalian-one-hybrid assay.
[b] The efficacy of the compounds on activation of PPARγ were measured by mammalian-one-hybrid assay.
[c] Compound binding to PPARγ was measured by fluorescence titration assay. All the values are expressed as the mean ± standard deviation (SD) from the dose-response curves of at least two independent experiments. Also see the Supplementary Figs. 1 and 2. TA, transcriptional activity.

assay (Table 1 and Supplementary Fig. 2), suggesting that the stronger ability of **2** in activating PPARγ came from its higher PPARγ binding affinity. These results indicated that the methyl sulfoxide group was not required or even detrimental for sulindac to transactivate and bind to PPARγ.

The methyl sulfoxide group is at the *para*-position of sulindac's benzylidene moiety. We then investigated whether chemical modification of this *para*-position with other functional groups could obtain optimization as to PPARγ modulation. Derivatives with fluorine (**3a**), isopropyl (**4a**), phenoxyl (**5a**) and benzyloxyl (**6a**) substitutions at the *para*-position were synthesized. We found that only the fluorine substituted derivative **3a** had comparable capability as **2** in activating (max fold induction: 3.18 ± 0.47) and binding to (K_D = 6.67 ± 0.65 μM) PPARγ. However, the other derivatives exhibited weaker capability (EC_{50} > 50 μM, max fold induction < 1.1 and K_D > 100 μM) (Table 1 and Supplementary Figs. 1 and 2), suggesting that chemical modifications at the *para*-position was indeed not appropriate for PPARγ-based optimization.

We then synthesized *meta*-substituted isomers (**3b**, **4b**, **5b**, **6b**) of above compounds. Surprisingly, all the four *meta*-substituted derivatives showed higher potency and efficacy ($EC_{50} \leq$ 6.41 μM, max fold induction ≥ 4.39) than their corresponding *para*-substituted isomers on transactivating Gal4/DBD-PPARγ/LBD (Table 1 and Supplementary Fig. 1). The *meta*- but not the *para*-substituted derivatives also substantially stimulated the transactivation of RXRα/PPARγ heterodimers (Fig. 1A). Consistently, the *meta*-substituted derivatives had higher PPARγ binding affinity ($K_D \leq$ 2.47 μM) (Table 1 and Supplementary Fig. 2). Hence, substitutions at the *meta*-rather than the *para*-position was favorable to PPARγ regulation.

To obtain SAR of *meta*-substitutions, we synthesized more *meta*-derivatives **7**-**10** with various substitutions (Table 1). However, all the derivatives had no obvious improvement in regulating and binding to PPARγ. We then explored the effect of *meta*-substitutions with large steric groups such as phenoxyl (**5b**) and benzyloxyl (**6b**). Surprisingly, **5b** and **6b** exhibited significantly higher potency and efficacy than **2** on activating and binding PPARγ (**5b**, EC_{50}: 1.178 ± 0.27 μM, max fold induction: 9.03 ± 0.40, and K_D = 1.73 ± 0.65 μM; **6b**, EC_{50}: 0.93 ± 0.44 μM, max fold induction: 10.26 ± 0.94, and K_D = 0.96 ± 0.35 μM) (Table 1 and Supplementary Figs. 1 and 2). Also, they had the strongest capability in activating PPARγ among all the synthesized *meta*-derivatives (Table 1 and Supplementary Fig. 1). The aromatic ring of phenoxyl and benzyloxyl moiety introduced in **5b** and **6b** formed π-π interaction with aromatic amino acid residues (His449) in the ligand binding pocket of PPARγ (Supplementary Fig. 4B and 4C), leading to enhanced binding energy. Hence, the derivatives with phenoxyl and benzyloxyl substitutions bound to PPARγ and likely induced a transactivating conformation of PPARγ.

It has been shown that sulindac derivatives with *E* benzylidene double bond are PPARγ ligands [25]. We then compared the PPARγ-based activity of the *E* and *Z* derivatives with methyl group at the *meta*-position of benzylidene moiety (**11_Z** and **11_E**). To obtain **11_E**, the methyl group in the indene moiety need to be removed to make the *E* configuration available. Interestingly, both **11_Z** and **11_E** activated and bound to PPARγ (Table 1 and Fig. 1B and Supplementary Figs. 1 and 2). Felts et al. reported that the *E* derivatives are mixed agonists of PPARγ and PPARα [25]. Consistently, we found that **11_E** activated both PPARα and PPARγ but not PPARβ (Fig. 2A). However, **11_Z** only activated PPARγ, but not PPARα or PPARβ (Fig. 2A). Moreover, all the *Z* derivatives that activated PPARγ did not activate PPARα or PPARβ (Fig. 2B), indicating the PPARγ selectivity of the *Z* derivatives. Thus, *Z* rather than *E* configuration rendered the derivatives with PPARγ selectivity. The advantage of the strict PPARγ selectivity of *Z* configuration is to avoid the PPARα-targeted side effects in the future clinical application.

We explored whether fluorine group in the indene moiety was essential for the derivatives to activate PPARγ. Mammalian-one-hybrid assay showed that **11_Z** and **11_E** could strongly induce PPARγ transactivation. However, their corresponding compounds **12_Z** and **12_E** without fluorine substitution failed to either bind to PPARγ or activate PPARγ (Table 1 and Fig. 1B and Supplementary Figs. 1 and 2). Thus, fluorine group in the indene moiety was vital for both the *Z* and *E* derivatives to activate and bind to PPARγ.

Moreover, we investigated the effect of **6b** on COX-2 activity in vitro. Sulindac sulfide exhibited strong potency on inhibiting COX-2 activity with an IC_{50} at 1.396 μM, whereas the potency of **6b** was much weaker (IC_{50}, 286.1 μM) (Supplementary Fig. 5), verifying previous reports that the methythiol group of sulindac sulfide is essential for COX inhibition.

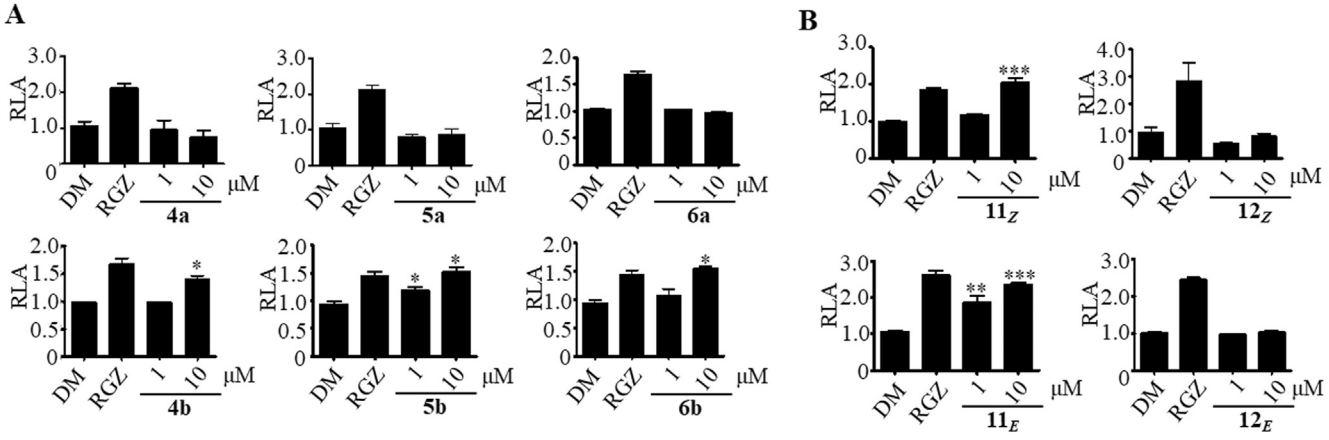

Fig. 1. Derivatives with *meta*-substitutions and fluorine activate the transcriptional activity of RXRα/PPARγ heterodimer. Cos-7 cells were co-transfected with PPRE-luciferase, renilla-luciferase, RXRα and PPARγ expression plasmids, and then treated with the indicated compounds for 12 h. Cells were then harvested, and firefly and renilla luciferase activities were measured. Renilla luciferase values were normalized to firefly luciferase activity to obtain the relative luciferase activity. DM, DMSO; RGZ, rosiglitazone (0.1 μM); RLA, relative luciferase activity. Data are presented as means ± SD. Statistical significance of differences of each condition vs. DMSO control was calculated by student's *t*-test. *p < 0.05, **p < 0.01, ***p < 0.001.

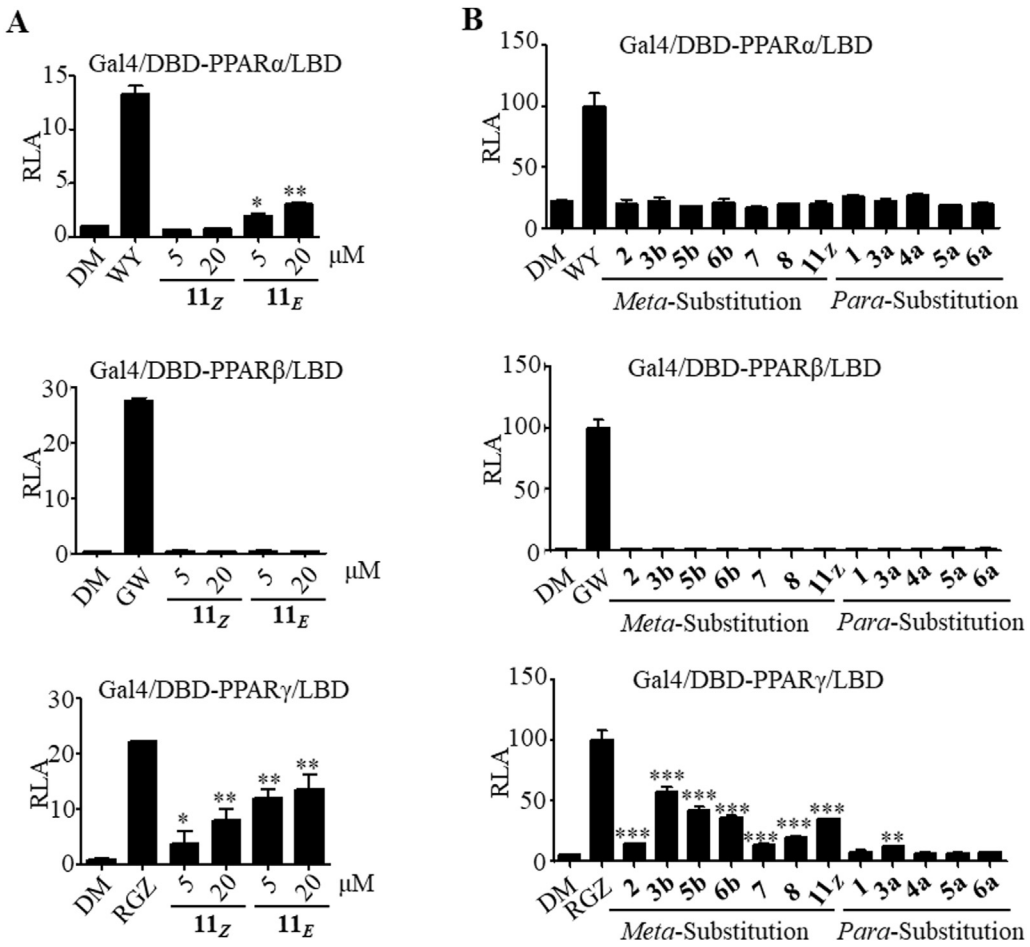

Fig. 2. Selective PPARγ activation by the *Z*-configured benzylidene compounds bearing a substituent in the *meta* position. HEK293T cells were co-transfected with pG5-luciferase and pBIND-PPARγ/LBD or pBIND-PPARα/LBD or pBIND-PPARβ/LBD plasmids. Cells were treated with the indicated compounds for 12 h. Renilla luciferase values were normalized to firefly luciferase activity to obtain the relative luciferase activity. The concentration of sulindac derivatives was 5 μM (B). WY, WY14643 (1 μM); RGZ, rosiglitazone (1 μM); GW, GW501516 (1 μM); RLA, relative luciferase activity. Data are presented as means ± SD. Statistical significance of differences of each condition vs. DMSO control was calculated by student's *t*-test. *p < 0.05, **p < 0.01, ***p < 0.001.

2.3. ***11Z*** *and* ***6b*** *weakly induced RXRα/PPARγ targeted gene expression and adipogenesis*

To further characterize the properties of sulindac derivatives as PPARγ ligands, we evaluated their adipogenic activity, one of the major physiological functions of PPARγ agonists [29–31]. To this end, we selected two derivatives **6b** and **11_Z** showing PPARγ agonistic activity, as well as derivative **6a** without apparent agonistic activity as a negative control. PPARγ agonist rosiglitazone (1 μM) induced substantial adipogenesis in mouse 3T3-L1 pre-adipocytes as indicated by the significant increase of Oil red O staining (Fig. 3A and 3B). As expected, **6b** and **11_Z** also induced adipocyte differentiation. However, they were much less potent than rosiglitazone in adipogenesis induction (Fig. 3A and 3B), correlating with their relatively low induction of PPARγ trans-activation (Fig. 2). Consistently, **6a** without apparent PPARγ agonistic activity did not show pro-adipogenic effect (Fig. 3A and 3B). **6b** was also less potent than rosiglitazone in upregulating the mRNA expressions of adipocyte lipid binding protein 2 (aP2) and PPARγ, two PPARγ targeted genes (Fig. 3C).

2.4. ***6b*** *improved hyperglycaemia in murine diabetes model*

The binding and activation of PPARγ prompted us to investigate the therapeutic effect of the derivatives on diabetes [10]. To this end, we selected **6b** because of its relatively high ability in PPARγ modulation. Compared with the control mice fed with normal diet, the high-fat-diet (HFD) model mice exhibited serious glucose intolerance, indicated by the continuous high level of glucose after glucose spike (Fig. 4A). Both rosiglitazone and **6b** significantly improved glucose tolerance, indicated by the reduced glucose level compared with the vehicle treatment group (Fig. 4A). The anti-diabetes effect of **6b** was further verified by its improvement of insulin resistance in our cell-based assay (Fig. 4B and 4C). High concentration of palmitic acid (PA) treatment impaired insulin signal in HepG2 cells, showing from reduced insulin-induced AKT phosphorylation [32–34]. **6b** and rosiglitazone potently enhanced insulin-induced AKT activation in this insulin-resistance cell model (Fig. 4B and 4C). Thus, **6b** might increase insulin sensitivity to improve glucose tolerance.

2.5. ***6b*** *and* ***11Z*** *had no significant effect on osteoblastic differentiation*

One of the adverse effects of rosiglitazone and other thiazolidinediones is the inhibition of osteoblastogenesis, resulting in osteoporosis from long-term usage [35–39]. As shown in Fig. 5A and 5B, the calcification, a marker of osteoblast, was strongly induced by inducing agents in rat osteosarcoma UMR106 cells as stained by Alizarin Red S. Rosiglitazone strongly reduced

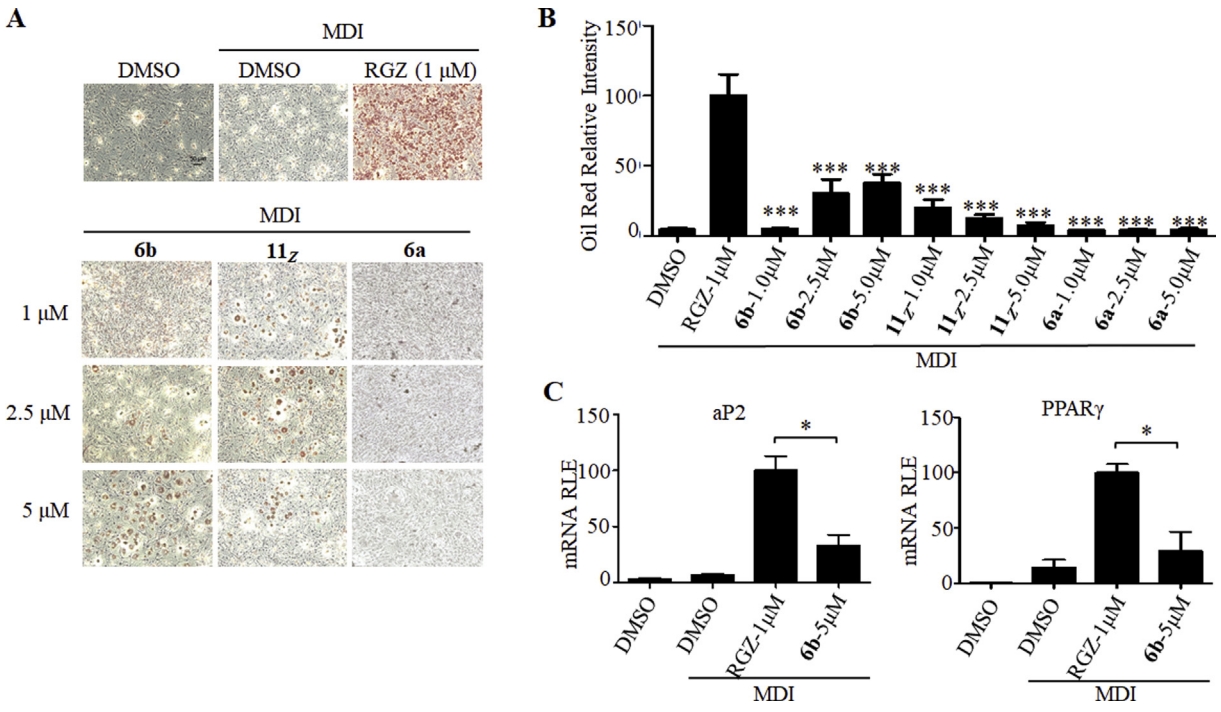

Fig. 3. **6b** and **11$_z$** have moderate adipogenetic effect. 3T3-L1 cells were cultured in the differentiated medium (MDI) containing 3-isobutyl-1-methylxanthine (5 mM), dexamethasone (1 μM) and insulin (10 μg/ml) with or without the compounds. (A) Lipid droplets and nuclei were stained with oil red and hematoxylin, respectively. Scale bar represents 50 μm. (B) The oil red intensity was measured and quantified by Image J software. (C) The expression of PPARγ-targeted genes (aP2 and PPARγ) was examined using qRT-PCR. RLE, relative expression. Data are presented as means ± SD. Statistical significance of differences of each condition vs. RGZ treatment was calculated by student's *t*-test. *p < 0.05, ***p < 0.001.

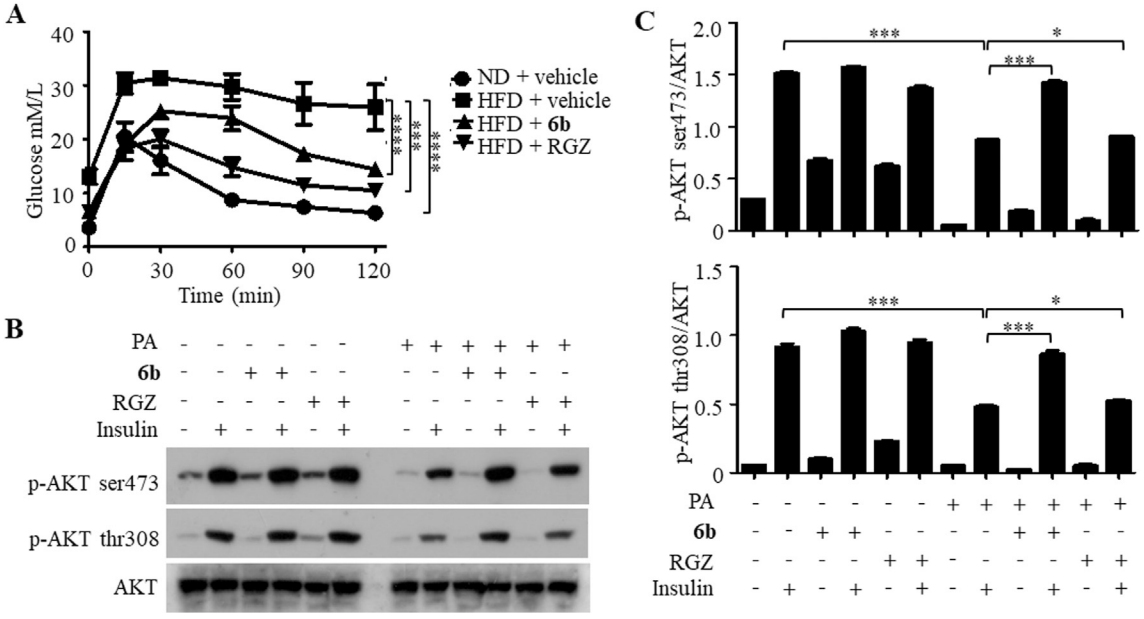

Fig. 4. **6b** Improves glucose tolerance. (A) The HFD-induced diabetes mice were treated with the vehicle or the compounds (4 mg/kg of rosiglitazone or 40 mg/kg of **6b**) for 1 month. The glucose tolerance test was performed. Statistical significance was calculated by Two-way ANOVA. (B, C) HepG2 cells treated with or without 200 mM palmitic acid for 24 h, and then co-treated with the indicated compounds (1 μM of rosiglitazone or 5 μM of **6b**) for 24 h. Cells were then treated with 10 nM of insulin for 15 min and harvested. Protein expression was detected by western blotting using anti-p-AKTser473, p-AKTthr308, AKT and β-actin antibodies. The expression of β-actin served as a loading control (B). The relative expression ratios of p-AKTthr308/AKT and p-AKTser473/AKT were measured by the Image J software (C). PA, palmitic acid; RGZ, rosiglitazone; ND, normal diet; HFD, high-fat-diet. Data are presented as means ± SD. *p < 0.05, ***p < 0.001, Student's *t*-test.

calcification in UMR106 cells (Fig. 5A and 5B). Also, the activity of alkaline phosphatase (ALP), a marker enzyme of osteoblast [40–42], was inhibited by rosiglitazone (Fig. 5C). These results verified that rosiglitazone inhibits osteoblastogenesis. In contrast to rosiglitazone, **6b** and **11$_z$** did not show inhibitory effect on mineralization and ALP activity at 5 μM concentration (Fig. 5), suggesting

their less adverse effect on osteoblastogenesis than rosiglitazone. Similar results were obtained by using mouse primary mesenchymal stem cells (Supplementary Fig. 6). These data were also in agreement with the lower agonistic activity of **6b** and **11$_Z$** than rosiglitazone (Fig. 2B). Hence, the derivatives of sulindac may avoid the adverse effect of potent PPARγ agonists on osteoblastogenesis. Moreover, we did not observe apparent effect of **6b** on HFD mouse weight (Supplementary Fig. 7).

2.6. Molecular docking study of **6b** to the ligand-binding pocket (LBP) of PPARγ

Molecular docking was utilized to uncover the binding modes of PPARγ with **6b** (**5b** for comparison). Since the crystal structures of sulindac sulfide/PPARγ-LBD (PDB ID: 4XUH) and rosiglitazone/PPARγ-LBD (PDB ID: 5YCP) have been reported [19,43], sulindac sulfide and rosiglitazone were selected as the reference binding modes. After molecular redocking to their corresponding binding pocket, the binding energies of sulindac sulfide and rosiglitazone were - 10.353 kcal mol $^{-1}$ and - 9.422 kcal mol $^{-1}$, respectively (Fig. 6A).

The 3D structure of **5b** and **6b** were established based upon the chemical structure of sulindac sulfide and then docked into the binding pocket of PPARγ randomly according to the Glide algorithm and optimized parameters. To our surprised, both **5b** and **6b** took a similar binding pattern as rosiglitazone but not as sulindac sulfide (Fig. 6 and Supplementary Figs. 3 and 4) with a reasonable binding energy (−8.448 kcal mol^{-1} for **5b** and −8.724 kcal mol^{-1} for **6b**). The binding pocket analysis showed that PPARγ-LBP could recruit two sulindac sulfides in the crystal complexes (PDB ID: 4XUH) (Fig. 6A). The introduction of the phenoxyl or benzyloxyl steric groups in the *meta*-position of sulindac scaffold would force **5b** and **6b** to assume different positions in the LBP in order to avoid steric clashes with protein residues and, in this case, unlike sulindac, only one molecule could occupy the LBP.

The carboxylic acid of sulindac sulfide (molecule 502) and thiazolidinedione moiety of rosiglitazone could form four hydrogen bonds with His449, Tyr473, His323 and Ser289 in the Y-shape pocket of PPARγ-LBP (Fig. 6B). Interestingly, the carboxylic acid group of **5b** and **6b** could not afford the same interaction with the four corresponding amino acid residues. Instead, they formed two hydrogen bonds with amides of Ser342 and Glu343. Meanwhile, their phenoxyl or benzyloxyl groups could stay close to the aromatic residues Tyr473, His323 and Tyr327 to form only additional hydrophobic interaction and construct a π-π stacking interaction towards His449 with a reasonable distance (4.61 Å for **6b** and 4.65 Å for **5b,** Supplementary Fig. 4B and 4C), without any classical hydrogen bonds in this pocket (Fig. 6B). **5b** and **6b** did not form any hydrogen bond with Tyr473, and thereby they could not stabilize the H12 of PPARγ effectively. This was in accordance with their property of weak agonists of PPARγ. Furthermore, the benzene ring of benzylidene moiety of **5b** and **6b** overlapped nicely with the benzene ring of rosiglitazone that would have a contact with Cys285, Met364 and Leu330. Thus, **5b** and **6b** represented an interesting binding mode with PPARγ-LBD, which was much different from sulindac sulfide.

2.7. Metabolic stability and pharmacokinetic study of **6b**

Metabolic stability of **6b** was determined in rat liver microsome. As shown in Fig. 7A, **6b** was stable in buffer, but decreased gradually over the microsome-incubation time period. It decreased by 40% after incubation with rat liver microsome for 90 min. The half-life ($T_{1/2}$) of **6b** and the clearance rate in rat liver microsome are

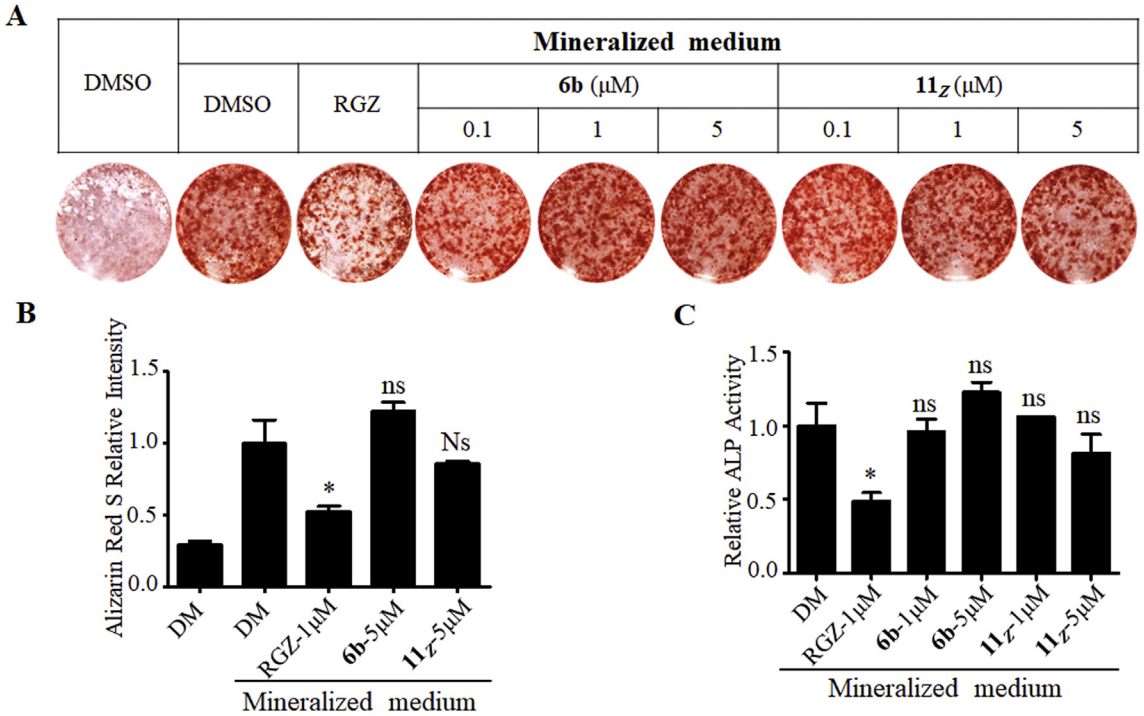

Fig. 5. Less osteoblastogenesis inhibition of **6b** and **11$_Z$**. UMR-106 cells were seeded into 96-well plates. Cells were then incubated with the mineralized medium containing 10 mM of β-glycerophosphate disodium salt hydrate and 50 μM of L-ascorbic acid with or without the compounds for 48 h. (A) Cells were fixed with 4% paraformaldehyde and stained with Alizarin Red S for 30 min. (B) Image J software was used to analyze and quantify the calcium deposition. (C) Activity of alkaline phosphatase was measure, and the values were normalized to total protein concentrations. RGZ, rosiglitazone; DM, DMSO; ALP, alkaline phosphatase. Data are presented as means ± SD. Statistical significance of differences of each condition vs. DMSO control was calculated by student's *t*-test. *p < 0.05, **p < 0.01, ***p < 0.001, ns: p > 0.05.

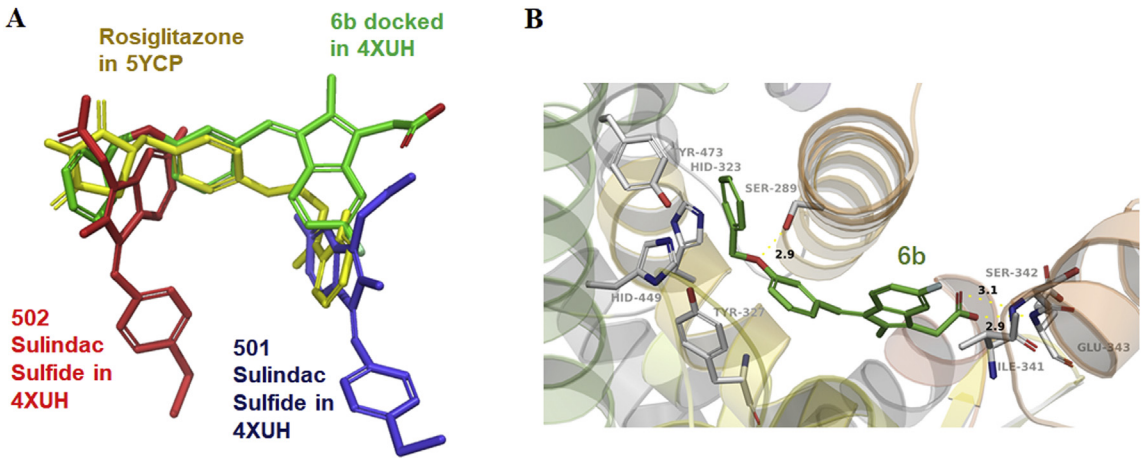

Fig. 6. Proposed binding mode of **6b** in comparison with sulindac sulfide and rosiglitazone in the crystal structure of ligand binding pocket (LBP) of PPARγ. (A) Overlapping of binding pose of sulindac sulfide (red for 502 and blue for 501 in 4xuh), rosiglitazone (yellow) and **6b** (green) in PPARγ-LBP. (B) Binding pose of **6b** (green) in PPARγ-LBP predicted by Glide SP.

117.45 min and 14.75 μL $min^{-1} \cdot mg^{-1}$, respectively. We further performed pharmacokinetic study of **6b** in rats. **6b** was administered by oral absorption (30 mg/kg) or intravenous injection (3 mg/kg), and the plasma concentrations of **6b** at different time points was measured (Fig. 7B and 7C). As shown in Table 2, **6b** exhibited a good oral bioavailability in rats (F = 97%). The maximal plasma concentration of **6b** reached 80.25 ± 8.66 mg/L at 1.5 h after oral administration and the elimination half-life in female rats was 4.75 ± 0.84 h.

3. Conclusion

Sulindac derivatives showed interesting PPARγ-based structural-activity relationship. As to PPARγ binding and activation, the *meta*-position substitution in the benzylidene moiety was much more effective than the *para*-position substitution. Unlike *E* derivatives, *Z* derivatives showed the PPARγ selectivity. Phenoxyl and benzyloxyl *meta*-substitutions endowed the derivatives with strong potency on regulation and binding of PPARγ. Indene fluorine

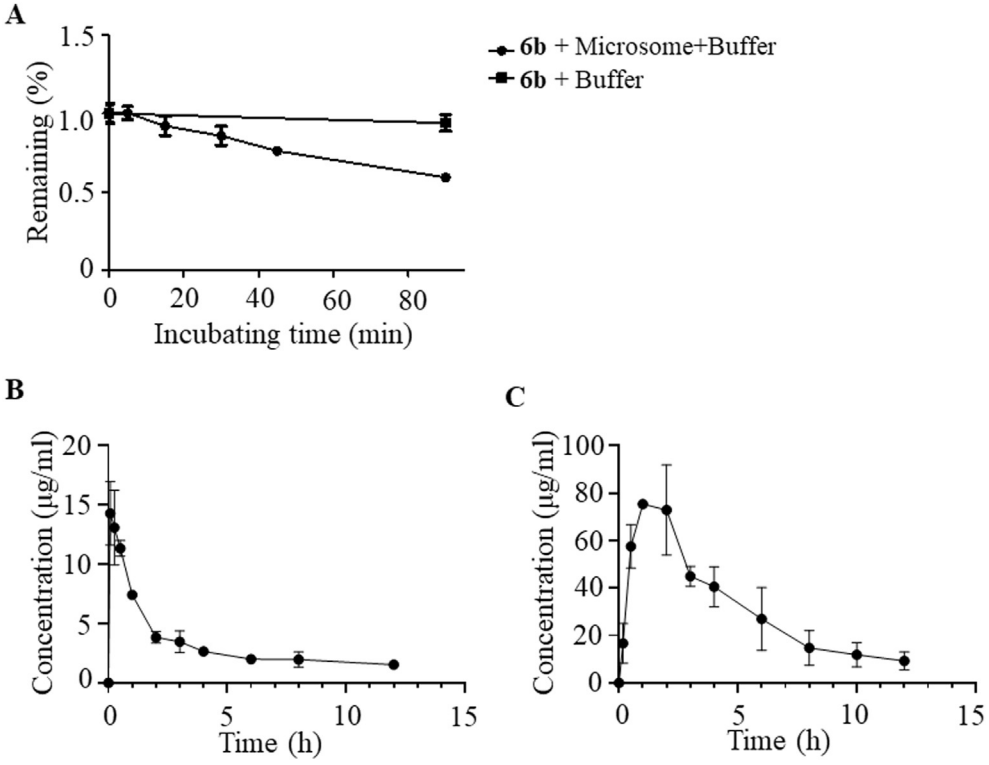

Fig. 7. Pharmacokinetic profiles of **6b**. (A) Stability of **6b** was examined using rat liver microsome. **6b** (40 μM) was incubated with microsome for different time, and the percentage of **6b** remaining amount to **6b** amount at 0 min was determined. Data are presented as means ± SEM, n = 3. (B, C) Plasma concentration-time profiles of **6b** in Sprague-Dawley (SD) rats after intravenous administration at 3 mg/kg (B) or oral administration at 30 mg/kg (C). Also see Table 2.

Table 2
Pharmacokinetic parameters of **6b** in rats.

Parameters	Unit	Oral (30 mg/kg)	IV (3 mg/kg)
AUC_{0-t}	mg/L*h	379.69 ± 98.32	39.30 ± 5.45
$AUC_{0-\infty}$	mg/L*h	444.53 ± 136.60	51.58 ± 11.31
$T_{1/2z}$	h	4.75 ± 0.84	7.06 ± 1.41
T_{max}	h	1.5 ± 0.71	-
V_z/F	L/kg	0.47 ± 0.06	0.59 ± 0.01
CL_z/F	L/h/kg	0.07 ± 0.02	0.06 ± 0.01
C_{max}	mg/L	80.25 ± 8.66	14.29 ± 2.67

AUC_{0-t}, area under the plasma concentration-time curve values of **6b** during 12 h; $AUC_{0-\infty}$, able to cover the total AUC; $T_{1/2z}$, terminal elimination half-life; T_{max}, the time to reach a peak concentration; V_z/F, distribution volume; CL_z/F, clearance; C_{max}, peak plasma concentration. Data are presented as mean ± SD, n = 2. Data was calculated by software DAS 3.2.8. Also see Fig. 7B and 7C.

was vital for the derivatives binding to PPARγ and regulating PPARγ transactivation. Hence, our results provide some useful guidance for designing sulindac derivatives targeting PPARγ.

6b exhibited strong anti-diabetic effect through improving insulin resistance. Compared with clinical drug rosiglitazone, the derivatives had less PPARγ transactivating activity, which may reduce the severe side effects from the potent induction of PPARγ-targeted genes. Indeed, **6b** and **11_Z** had no obvious effect on inhibiting osteoblastic differentiation and had relatively low effect on adipogenic induction. Thus, the *meta*-substitution and *Z* configuration derivatives of sulindac may be the next generation of PPARγ-targeting drugs for diabetes.

4. Experimental

4.1. Chemistry

General synthesis of indene **Rec1** and **Rec2**.

Zn (320 mg, 5 mmol) was placed in a 50 mL two-necked round bottom flask which was evacuated and flushed with nitrogen and then 12 mL THF was added as solvent. Ethyl bromoacetate (350 mg, 2.1 mmol) was added dropwise, followed by a catalytic amount of I_2 to initiate the reaction. Different indenone (164 mg,1 mmol) was added dropwise, and after 30 min, the reaction was refluxed for 4 h. After quenching reaction by HCl (10%, 10 mL), the mixture was extracted with Et_2O (3 × 20 mL) and washed with water (3 × 10 mL). The combined organic layers were dried and concentrated under vacuum. To the residue, NaOH (1 N, 10 mL) and MeOH (6.7 mL) was added. After stirring overnight at room temperature, the mixture was quenched by HCl (20%, 2.5 mL). The aqueous solution was extracted with EtOAc (3 × 15 mL). The combined extracts were dried over Na_2SO_4 and concentrated under reduced pressure. The residue was purified by flash column chromatography on *silica gel* (ethyl acetate: PE = 1 : 10) to afford compound **Rec1** and **Rec2**.

General procedure for the synthesis of sulindac derivatives. Using MeONa as the base catalyst and MeOH as the solvent, indene could react with different substituted aromatic aldehydes to construct structurally diverse sulindac analogues with moderate yields for the following SAR study (see Scheme 1).

4.1.1. (Z)-2-(5-fluoro-1-(4-fluorobenzylidene)-2-methyl-1H-inden-3-yl) acetic acid (**3a**)

Yellow solid; M.p. 184–187 °C. ^{1}H NMR (600 MHz, DMSO-d_6) δ = 12.42 (br. s., 1H), 7.58 (dd, *J* = 5.7, 8.3 Hz, 2H), 7.31–7.35 (m, 3H), 7.17 (dd, *J* = 5.1, 8.4 Hz, 1H), 7.02 (dd, *J* = 2.4, 9.2 Hz, 1H), 6.73 (dt, *J* = 2.4, 8.9 Hz, 1H), 3.57 (s, 2H), 2.15 (s, 3H); ^{13}C NMR (151 MHz, DMSO-d_6) δ = 172.06, 163.45 (d, *J* = 68.2 Hz), 161.86 (d, *J* = 71.5 Hz), 147.41 (d, *J* = 8.8 Hz), 140.09, 138.36, 132.93, 132.91, 132.53, 131.80 (d, *J* = 8.8 Hz, 2C), 130.31, 129.97, 123.48 (d, *J* = 8.8 Hz), 116.11 (d, *J* = 22.0 Hz), 110.79 (d, *J* = 23.1 Hz), 106.40 (d, *J* = 23.1 Hz), 31.55, 10.70. HRMS (ESI) calcd for $C_{19}H_{14}F_2NaO_2^+$ [M+Na^+]: 335.0854; found: 335.0857. HPLC purity: 98.54%.

4.1.2. (Z)-2-(5-fluoro-1-(3-fluorobenzylidene)-2-methyl-1H-inden-3-yl) acetic acid (**3b**)

Yellow solid; yield 74%; M.p.182–183 °C; ^{1}H NMR (600 MHz, $CDCl_3$) δ = 7.41 - 7.35 (m, 1H), 7.26 (d, *J* = 8.4 Hz, 1H), 7.17 (d, *J* = 7.9 Hz, 2H), 7.12 (s, 1H), 7.07 (t, *J* = 8.3 Hz, 1H), 6.87 (d, *J* = 8.8 Hz, 1H), 6.57 (t, *J* = 8.7 Hz, 1H), 3.57 (s, 2H), 2.18 (s, 3H); ^{13}C NMR (151 MHz, $CDCl_3$) δ = 176.64, 163.28 (d, *J* = 246.5 Hz, 1C), 162.78 (d, *J* = 246.5 Hz, 1C), 146.35 (d, *J* = 8.8 Hz, 1C), 141.07, 138.73 (d, *J* = 7.7 Hz, 1C), 138.67, 130.74, 130.13 (d, *J* = 7.7 Hz, 1C), 129.50 (d, *J* = 2.2 Hz, 1C), 128.84, 125.00 (d, *J* = 2.2 Hz, 1C), 123.87 (d, *J* = 8.8 Hz, 1C), 116.03 (d, *J* = 22.0 Hz, 1C), 115.11 (d, *J* = 19.8 Hz, 1C), 110.87 (d, *J* = 23.1 Hz, 1C), 105.96 (d, *J* = 23.1 Hz, 1C), 31.42, 10.52; HRMS (ESI) calcd for $C_{19}H_{14}F_2NaO_2^+$ [M+Na^+]: 335.0854; found: 335.0849. HPLC purity: 98.41%.

4.1.3. (Z)-2-(5-fluoro-1-(3-isopropylbenzylidene)-2-methyl-1H-inden-3-yl) acetic acid (**4b**)

Yellow solid; yield 77%; M.p. 130–131 °C. ^{1}H NMR (600 MHz, $CDCl_3$) δ = 7.40 (s, 1H), 7.35 (t, *J* = 7.7 Hz, 1H), 7.32 - 7.28 (m, 2H), 7.24 - 7.21 (m, 2H), 6.88 (dd, *J* = 2.4, 9.0 Hz, 1H), 6.55 (dt, *J* = 2.4, 8.8 Hz, 1H), 3.59 (s, 2H), 2.93 (spt, *J* = 6.9 Hz, 1H), 2.21 (s, 3H), 1.27 (d, *J* = 7.0 Hz, 6H). ^{13}C NMR (151 MHz, $CDCl_3$) δ = 176.23, 163.11 (d, *J* = 245.4 Hz, 1C), 149.01, 146.22 (d, *J* = 8.8 Hz, 1C), 140.02, 138.88, 136.36, 131.22, 129.97 (d, *J* = 2.2 Hz, 1C), 129.85 (d, *J* = 2.2 Hz, 1C), 128.49, 127.57, 126.70, 126.59, 123.88 (d, *J* = 8.8 Hz, 1C), 110.56 (d, *J* = 23.1 Hz, 1C), 105.68 (d, *J* = 24.2 Hz, 1C), 34.16, 31.41, 23.94 (s, 2C), 10.59. HRMS (ESI) calcd for $C_{22}H_{21}FNaO_2^+$ [M+Na^+]: 359.1417; found: 359.1418. HPLC purity: 99.56%.

4.1.4. (Z)-2-(5-fluoro-2-methyl-1-(4-phenoxybenzylidene)-1H-inden-3-yl) acetic acid (**5a**)

Yellow solid; yield 65%; M.p.154–155 °C; ^{1}H NMR (600 MHz, $CDCl_3$) δ = 7.47 (d, *J* = 8.6 Hz, 2H), 7.35–7.41 (m, 3H), 7.14–7.18 (m, 2H), 7.08–7.12 (m, 2H), 7.04 (d, *J* = 8.4 Hz, 2H), 6.88 (dd, *J* = 8.9, 2.1 Hz, 1H), 6.59 (td, *J* = 8.8, 2.2 Hz, 1H), 3.58 (s, 2H),2.20 (s, 3H); ^{13}C NMR (151 MHz, $CDCl_3$) δ = 176.3, 163.1 (d, *J* = 247.6 Hz), 157.7, 156.5, 146.2 (d, *J* = 8.8 Hz), 139.8, 138.9, 131.1 (2C), 130.2, 129.9 (2C), 129.9 (d, *J* = 2.2 Hz), 129.7 (d, *J* = 2.2 Hz), 123.9, 123.7 (d, *J* = 8.8 Hz), 119.5 (2C), 118.3 (2C), 110.7 (d, *J* = 23.1 Hz), 105.8 (d, *J* = 23.1 Hz), 31.4, 29.7, 10.6; HRMS (ESI) calcd for $C_{25}H_{19}FNaO_3^+$ [M+Na^+]: 409.1210; found: 409.1203.

4.1.5. (Z)-2-(5-fluoro-2-methyl-1-(3-phenoxybenzylidene)-1H-inden-3-yl) acetic acid (**5b**)

Yellow solid; yield 53%; M.p.110–112 °C; ^{1}H NMR (600 MHz, $CDCl_3$) δ = 7.38 (t, *J* = 7.9 Hz, 1H), 7.36 - 7.32 (m, 2H), 7.26 (dd, *J* = 5.2, 8.3 Hz, 1H), 7.22 (d, *J* = 7.5 Hz, 1H), 7.13 (s, 1H), 7.12 - 7.08 (m, 2H), 7.06 - 7.02 (m, 3H), 6.85 (dd, *J* = 2.4, 8.8 Hz, 1H), 6.56 (dt, *J* = 2.5, 8.8 Hz, 1H), 3.55 (s, 2H), 2.16 (s, 3H); ^{13}C NMR (151 MHz, $CDCl_3$) δ = 176.62, 163.23 (d, *J* = 246.5 Hz, 1C), 157.67, 156.92, 146.30 (d, *J* = 8.8 Hz, 1C), 140.60, 138.82, 138.28, 130.43, 129.94, 129.92 (s, 2C), 129.82, 129.64 (d, *J* = 2.2 Hz, 1C), 124.15, 123.97 (d, *J* = 8.8 Hz, 1C), 123.70, 119.28 (s, 2C), 119.24, 118.72, 110.76 (d, *J* = 22.0 Hz, 1C), 105.87 (d, *J* = 24.2 Hz, 1C), 31.45, 10.59. HRMS (ESI)calcd for $C_{25}H_{19}FNaO_3^+$ [M+Na^+]: 409.1210; found: 409.1205. HPLC purity: 98.47%.

4.1.6. (Z)-2-(1-(4-(benzyloxy)benzylidene)-5-fluoro-2-methyl-1H-inden-3-yl) acetic acid (**6a**)

Yellow solid; yield 35%; M.p.135–136 °C; ^{1}H NMR (600 MHz, DMSO-d_6) δ = 7.51 (d, *J* = 8.6 Hz, 2H), 7.49 (d, *J* = 7.2 Hz, 2H), 7.44 -

7.40 (m, 2H), 7.40 - 7.34 (m, 2H), 7.30 (s, 1H), 7.14 (d, J = 8.6 Hz, 2H), 7.01 (dd, J = 2.6, 9.4 Hz, 1H), 6.73 (dt, J = 2.4, 8.9 Hz, 1H), 5.18 (s, 2H), 3.57 (s, 2H), 2.15 (s, 3H); ^{13}C NMR (151 MHz, $CDCl_3$) δ = 175.51, 163.02 (d, J = 246.5 Hz, 1C), 158.93, 146.16 (d, J = 8.8 Hz, 1C), 139.30, 138.95, 136.70, 130.98 (s, 2C), 130.71, 129.84 (d, J = 2.2 Hz, 1C), 129.61 (d, J = 2.2 Hz, 1C), 128.98, 128.67 (s, 2C), 128.13, 127.56 (s, 2C), 123.61 (d, J = 8.8 Hz, 1C), 114.84 (s, 2C), 110.56 (d, J = 23.1 Hz, 1C), 105.62 (d, J = 23.1 Hz, 1C), 70.12, 31.30, 10.61. HRMS (ESI) calcd for $C_{26}H_{21}FNaO_3^+$ [M+Na$^+$]: 423.1367; found: 423.1359.

4.1.7. (Z)-2-(1-(3-(benzyloxy)benzylidene)-5-fluoro-2-methyl-1H-inden-3-yl) acetic acid (**6b**)

Yellow solid; yield 73%; M.p.169–171 °C; ^{1}H NMR (600 MHz, $CDCl_3$) δ = 7.40–7.44 (m, 2H), 7.37 (t, J = 7.4 Hz, 2H), 7.30–7.35 (m, 2H), 7.22–7.28 (m, 1H), 7.17 (s, 1H), 7.06–7.12 (m, 2H), 6.99 (dd, J = 8.3, 2.2 Hz, 1H), 6.86 (dd, J = 8.8, 2.2 Hz, 1H), 6.53 (td, J = 8.8, 2.3 Hz, 1H), 5.06 (s, 2H) 3.57 (s, 2H), 2.19 (s, 3H); ^{13}C NMR (151 MHz, $CDCl_3$) δ = 176.6, 163.1 (d, J = 246.5 Hz), 158.8, 146.2 (d, J = 8.8 Hz), 140.4, 138.8, 137.9, 136.8, 130.4, 130.2 (d, J = 2.2 Hz), 129.7 (d, J = 3.3 Hz), 129.7, 128.6 (2C), 128.1, 127.5 (2C), 124.0 (d, J = 8.8 Hz), 122.0, 115.2, 115.1, 110.8 (d, J = 22.0 Hz), 105.8 (d, J = 23.1 Hz), 70.0, 31.4, 10.6; HPLC purity: 99.81%.

4.1.8. (Z)-2-(1-(3-bromobenzylidene)-5-fluoro-2-methyl-1H-inden-3-yl) acetic acid (**7**)

Yellow solid; yield 70%; M.p.163–163 °C. ^{1}H NMR (600 MHz, $CDCl_3$) δ = 7.64 (s, 1H), 7.51 (d, J = 8.1 Hz, 1H), 7.42 (d, J = 7.7 Hz, 1H), 7.28–7.33 (m, 1H), 7.17 (dd, J = 8.4, 5.1 Hz, 1H), 7.11 (s, 1H), 6.88 (dd, J = 8.8, 2.4 Hz, 1H), 6.59 (td, J = 8.8, 2.4 Hz, 1H), 3.59 (s, 2H), 2.19 (s, 3H); ^{13}C NMR (151 MHz, $CDCl_3$) δ = 175.6, 163.3 (d, J = 246.5 Hz), 146.4 (d, J = 8.8 Hz),141.2, 138.7, 138.6, 132.0, 131.1, 130.9, 130.1, 129.5, 128.5, 127.8, 123.8 (d, J = 8.8 Hz), 122.6, 110.9 (d, J = 22.0 Hz), 106.0 (d, J = 24.2 Hz), 31.3, 10.5; HRMS (ESI) calcd for $C_{19}H_{14}BrFNaO_2^+$ [M+Na$^+$]: 395.0053; found: 395.0047. HPLC purity: 98.72%.

4.1.9. (Z)-2-(1-(3-chlorobenzylidene)-5-fluoro-2-methyl-1H-inden-3-yl) acetic acid (**8**)

Yellow solid; yield 75%; M.p.162–163 °C. ^{1}H NMR (600 MHz, $CDCl_3$) δ = 7.47 (s, 1H), 7.33–7.39 (m, 3H), 7.16 (dd, J = 8.3, 5.0 Hz, 1H), 7.11 (s, 1H), 6.88 (dd, J = 8.8, 2.0 Hz, 1H), 6.58 (td, J = 8.8, 2.1 Hz, 1H), 3.58 (s, 2H),2.19 (s, 3H); ^{13}C NMR (151 MHz, $CDCl_3$) δ = 175.8, 163.3 (d, J = 244.3 Hz), 146.4 (d, J = 8.8 Hz), 141.2, 138.6, 138.4, 134.5, 130.8, 129.8, 129.5 (d, J = 2.2 Hz), 129.1, 128.6, 128.2, 127.4, 123.8 (d, J = 8.8 Hz), 110.9 (d, J = 23.1 Hz), 106.0 (d, J = 23.1 Hz), 31.3, 10.5; HRMS (ESI) calcd for $C_{19}H_{14}ClFNaO_2^+$ [M+Na$^+$]: 351.0559; found: 351.0553. HPLC purity: 99.32%.

4.1.10. (Z)-2-(5-fluoro-1-(3-hydroxybenzylidene)-2-methyl-1H-inden-3-yl) acetic acid (**9**)

Yellow solid; yield 45%; M.p. 172–177 °C. ^{1}H NMR (600 MHz, DMSO-d_6) δ = 9.64 (br. s., 1H), 7.30 - 7.27 (m, 3H), 7.01 (dd, J = 2.5, 9.3 Hz, 1H), 6.93 (d, J = 8.1 Hz, 1H), 6.92 (s, 1H), 6.82 (dd, J = 2.3, 8.2 Hz, 1H), 6.74 (dt, J = 2.4, 9.0 Hz, 1H), 3.57 (s, 2H), 2.14 (s, 3H); ^{13}C NMR (151 MHz, DMSO-d_6) δ = 172.11, 162.80 (d, J = 243.2 Hz, 1C), 157.87, 147.29 (d, J = 8.8 Hz, 1C), 139.75, 138.39, 137.81, 132.27 (d, J = 2.2 Hz, 1C), 131.60, 130.15, 130.08 (d, J = 2.2 Hz, 1C), 123.80 (d, J = 8.8 Hz, 1C), 120.22, 116.04, 115.87, 110.66 (d, J = 23.1 Hz, 1C), 106.24 (d, J = 23.1 Hz, 1C), 31.55, 10.71. HRMS (ESI) calcd for $C_{19}H_{16}FO_3^+$ [M+H$^+$]: 311.1078; found: 311.1078. HPLC purity: 97.34%.

4.1.11. (Z)-2-(5-fluoro-1-(3-methoxybenzylidene)-2-methyl-1H-inden-3-yl) acetic acid (**10**)

Yellow solid; yield 43%; M.p. 131–133 °C. ^{1}H NMR (600 MHz, DMSO-d_6) δ = 7.41 (t, J = 7.9 Hz, 1H), 7.34 (s, 1H), 7.25 (dd, J = 5.3, 8.4 Hz, 1H), 7.10 (d, J = 7.7 Hz, 1H), 7.08 (s, 1H), 7.03 - 6.97 (m, 2H), 6.73 (dd, J = 2.4, 8.1 Hz, 1H), 3.78 (s, 3H), 3.58 (s, 2H), 2.15 (s, 3H); ^{13}C NMR (151 MHz, DMSO-d_6) δ = 172.10, 162.85 (d, J = 243.2 Hz, 1C), 159.70, 147.37 (d, J = 8.8 Hz, 1C), 140.02, 138.35, 137.93, 132.48 (d, J = 2.2 Hz, 1C), 131.23, 130.20, 130.04 (d, J = 2.2 Hz, 1C), 123.74 (d, J = 8.8 Hz, 1C), 121.80, 114.70, 114.59, 110.71 (d, J = 23.1 Hz, 1C), 106.34 (d, J = 24.2 Hz, 1C), 55.60, 31.56, 10.70. HRMS (ESI) calcd for $C_{20}H_{17}FNaO_3^+$[M+Na$^+$]: 347.1054; found: 347.1056.

4.1.12. (Z)-2-(5-fluoro-2-methyl-1-(3-methylbenzylidene)-1H-inden-3-yl) acetic acid (**11$_Z$**)

Yellow solid; yield 63%; M.p.142–144 °C. ^{1}H NMR (600 MHz, $CDCl_3$) δ = 7.29 (m, 3H), 7.24–7.27 (m, 1H), 7.15–7.19 (m, 2H), 6.86 (d, J = 8.8 Hz, 1H), 6.54 (t, J = 8.7 Hz, 1H), 3.56 (s, 2H), 2.37 (s, 3H),2.18 (s, 3H); ^{13}C NMR (151 MHz, $CDCl_3$) δ = 177.0, 163.1 (d, J = 249.8 Hz), 146.2 (d, J = 8.8 Hz), 140.1, 138.9, 138.2, 136.5, 131.0, 130.0, 129.9, 129.0, 128.5 (d, J = 4.4 Hz), 128.4, 126.4, 123.9 (d, J = 8.8 Hz), 110.7 (d, J = 22.0 Hz), 105.7 (d, J = 23.1 Hz), 31.5, 21.4, 10.6; HRMS (ESI) calcd for $C_{20}H_{17}FNaO_2^+$ [M+Na$^+$]: 331.1105; found: 331.1100. HPLC purity: 97.86%.

4.1.13. (E)-2-(5-fluoro-1-(3-methylbenzylidene)-1H-inden-3-yl) acetic acid (**11$_E$**)

Yellow solid; ^{1}H NMR (600 MHz, $CDCl_3$) δ = 7.58 (dd, J = 5.0, 8.3 Hz, 1H), 7.38 - 7.34 (m, 3H), 7.30 (t, J = 7.5 Hz, 1H), 7.15 (d, J = 7.3 Hz, 1H), 7.04 (s, 1H), 7.01 (dd, J = 2.2, 8.8 Hz, 1H), 6.92 (dt, J = 2.2, 8.7 Hz, 1H), 3.66 (s, 2H), 2.39 (s, 3H); ^{13}C NMR (151 MHz, $CDCl_3$) δ = 176.37, 163.00 (d, J = 246.5 Hz, 1C), 143.11 (d, J = 8.8 Hz, 1C), 138.42, 137.93 (d, J = 2.2 Hz, 1C), 137.60, 136.58, 133.58 (d, J = 3.3 Hz, 1C), 130.84, 129.45, 129.24, 128.69, 127.32, 127.05, 120.08 (d, J = 8.8 Hz, 1C), 112.06 (d, J = 23.1 Hz, 1C), 106.64 (d, J = 24.2 Hz, 1C), 33.86, 21.47. HRMS (ESI) calcd for $C_{19}H_{15}FNaO_2$+ [M+Na$^+$]: 317.0948; found: 317.0945.

4.1.14. (Z)-2-(2-methyl-1-(3-methylbenzylidene)-1H-inden-3-yl) acetic acid (**12$_Z$**)

Yellow solid; yield 21%; ^{1}H NMR (600 MHz, $CDCl_3$) δ = 7.36 (d, J = 7.7 Hz, 1H), 7.33 (s, 1H), 7.33 - 7.29 (m, 2H), 7.20 (s, 1H), 7.18 (d, J = 7.2 Hz, 2H), 7.16 (d, J = 7.9 Hz, 1H), 6.89 (dt, J = 1.3, 7.5 Hz, 1H), 3.61 (s, 2H), 2.38 (s, 3H), 2.19 (s, 3H); ^{13}C NMR (151 MHz, $CDCl_3$) δ = 176.69, 143.88, 141.16, 138.05, 136.80, 136.74, 134.13, 130.99, 130.86, 129.93, 128.83, 128.33, 127.83, 126.38, 124.61, 122.87, 117.99, 31.46, 21.40, 10.48.

4.1.15. (E)-2-(1-(3-methylbenzylidene)-1H-inden-3-yl) acetic acid (**12$_E$**)

Yellow solid, ^{1}H NMR (600 MHz, $CDCl_3$) δ = 7 7.69 (d, J = 7.2 Hz, 1H), 7.44 (s, 1H), 7.39–7.42 (m, 2H), 7.31–7.34 (m, 2H), 7.29 (d, J = 9.0 Hz, 1H), 7.27 (d, J = 4.8 Hz, 1H), 7.15 (d, J = 7.5 Hz, 1H), 7.00 (s, 1H), 3.71 (s, 2H), 2.40 (s, 3H); ^{13}C NMR (151 MHz, $CDCl_3$) δ = 176.14, 141.29, 139.00, 138.64, 138.33, 137.95, 136.81, 130.86, 129.26, 128.71, 128.64, 127.43, 127.35, 125.57, 125.25, 119.10, 119.04, 33.89, 21.47. HRMS (ESI) calcd for $C_{19}H_{15}O_2^-$ [M$^-$]: 275.1078; found: 275.1081.

4.2. Materials for biological assays

Insulin (I9278), dexamethasone (D2915), IBMX (I5879), β-Glycerophosphate disodium salt hydrate (G9422), L-ascorbic acid (A4544), D-(+)-Glucose (G7021), WY-14643 (C7081), GW501516 (43732), rosiglitazone (R2408), Oil Red O (O0625) Solutol HS 15 (70142-34-6), and Alizarin Red S (A5533) were purchased from Sigma-Aldrich; Alkaline phosphatase Kit (P0321) and COX-2 enzyme immune assay kit (S0168) were purchased from Beyotime Biotechnology (China). IPTG Dioxane Free (A600168) and Imidazole (A600277) were purchased from Sangon Biotech (China).

Glycerol was purchased from Sinopharm Chemical Reagent Co. Ltd. PPRE-Luc, pG5-luc, pcmv-myc-RXRα, pcmv-myc-PPARγ, pBind-PPARγLBD, pBind-PPARαLBD, pBind-PPARβLBD and pCMV-renilla plasmids were cloned by our lab. Phospho-Akt Ser473 (#4060) and Phospho-Akt Thr308 (#13038) were purchased from cell Signaling Technology. AKT1/2/3 (H-136) antibody was purchased from Santa Cruz. β-actin (A5441) antibody was purchased from Sigma-Aldrich. One touch Ultra Easy and Blood glucose test strips were purchased from LifeScan Inc. TRIzol LS Reagent (10296-010) was purchased from life technology. FastStart Universal SYBR Green Master (Rox) (4913850001) was purchased from Roche. Phosphate buffer (451201) and rat liver microsome (452511) were purchased from Corning.

4.3. Molecular docking and structural comparison

The chemical structures of **5b** and **6b** were constructed based upon the 502 molecule (Sulindac sulfide) in protein complex (PDBID: 4XUH). 64 conformations of **5b** were generated by Confgen module in Schrodinger suite and then docked into the PPARγ binding site by Glide-HTVS and SP method, respectively. The parameters were set as that: Gridcenter on 502 molecule and GridBox was 10 Å. 128 conformations of **6b** were generated and similar docking was done. Two sulindac sulfide in protein complex (PDBID: 4XUH) named 502 and 501 were selected as reference compounds. Also, rosiglitazone in protein complex (PDBID: 5YCP) was chosen for comparison. All the figures were generated by Schrodinger suite or PyMol software.

4.4. Mammalian one-hybrid assay (pBind system reporter assay)

HEK293T cells were co-transfected with pG5-luc (Promega) and pBind-PPARγ/LBD, pBind-PPARα/LBD, or pBind-PPARβ/LBD plasmid at cell density of 60−80%. After 24 h, cells were treated with the compounds or the PPAR positive agonists (rosiglitazone, WY-14643 or GW501516) for 12 h. Cells were lysed by Promega passive lysis buffer, and the fluorescence values of luciferase and Renilla were measured by Promega Microplate Reader. Renilla luciferase values were normalized to firefly luciferase activity to obtain the relative luciferase activity for plotting.

4.5. PPRE-luciferase reporter assay

Cos-7 cells seeded at 24-well plates were co-transfected with PPRE-Luc (addgene), pCMV-myc-RXRα, pCMV-myc-PPARγ and pCMV-renilla plasmids. After 24 h, cells were treated with the compounds for 12 h. Cells were then collected and lysed with Promega passive lysis buffer. The fluorescence values of luciferase and renilla were measured by Promega Microplate Reader. Renilla luciferase values were normalized to firefly luciferase activity to obtain the relative luciferase activity for plotting.

4.6. PPARγ-LBD protein purification

The DNA fragment encoding amino acid sequence (237−504) of PPARγ/LBD was cloned into the expression vector pET-15b. Recombinant plasmid was transformed into *E. coli* (BL21 DE3 strain) and protein expression was induced by 1 mM isopropyl β-D-1-thiogalactopyranoside (IPTG) at 16 °C for 8 h. PPARγ-LBD protein was purified by nickel column using Akta avant instrument. The running buffer for purification was buffer A (25 mM Tris, 150 mM NaCl, 25 mM imidazole, 10% glycerol, [pH 7.5]). The elution buffer was buffer B (25 mM Tris, 500 mM imidazole, 10% glycerol, [pH 7.5]).

4.7. Fluorescence titration assay

Fluorescence titration was implemented on CARY ECLIPS spectra-fluorophotometer (Varian, USA). Data collection was ranged from 290 to 500 nm upon excitation at 282 nm for PPARγ. Excitation and emission bandwidths were all 5 nm. A 3 cm quartz cell was used for measurements. Reactions were all initiated by stepwise adding a little aliquot volume of ligand into 3.0 mL titrand at 25 °C. In this study, PPARγ was prepared in PBS buffer to give working concentrations of 3 μM to provide an optimal fluorescence peak. Solution of ligand was 2000 times higher than PPAR's to ensure the final ratio of ligand to titrand as “5”. Ligands were injected by 1:1000 into solution of PPARγ for each titration, blended after each injection, and the three times numerical reading in succession was required to guarantee the system stabilization. Furthermore, to be a control, PBS buffer with isometric DMSO is introduced to duplicate the whole process as ligand, to exclude the nonspecific quenching. Data fitting was executed on OriginPro 2016 (Origin, Inc), and the one site binding analysis for spectrum titration experiment according to literature was employed here to determine the dissociation constant (K_D) [44].

4.8. 3T3-L1 adipocyte formation assay

3T3-L1 cell seeded at 24-well plate were cultured for 2 days after confluence. Culture medium was replaced with fresh medium containing differentiation agent (5 mM 3-Isobutyl-1-methylxanthine, 1 μM dexamethasone and 10 μg/ml Insulin) and the testing compounds. After 48 h, cells were treated with fresh medium containing 10 μg/ml insulin for another 48 h and then a fresh medium for 72 h. Lipid droplets and nuclei were stained with oil red and hematoxylin, respectively [45,46].

4.9. Glucose tolerance test

C57/B6 mice were fed with high-fat diet for 3 months to make the concentration of fasting blood glucose more than 11.1 mM. The mice were then fed with compounds **6b** (40 mg/kg) or rosiglitazone (4 mg/kg) for another 1 month. The glucose tolerance test was carried out according to the reported literature. All experiments involving animals followed the approved protocols by the Laboratory Animal Center in Xiamen University.

4.10. Mineralization of UMR106 cells

UMR106 cells were seeded into 96-well plates for 48 h. Cells were then induced with mineralized medium (10 mM of β-Glycerophosphate disodium salt hydrate and 50 μM of L-ascorbic acid) in the presence or absence of the compounds. After 48 h, cells were fixed with 4% paraformaldehyde and washed with PBS twice, and then stained with Alizarin Red S for 30 min. Analysis of calcium deposition was performed by software Image J [42].

4.11. Osteoblastogenesis assay using mesenchymal stem cells

Mesenchymal stem cells were obtained from mouse bone marrow. Cells were cultured in α-MEM medium supplemented with 10% FBS, 2 mM glutamine, 100 U/ml penicillin, and 100 mg/ml streptomycin. Nonadherent cells were removed after 24 h, and adherent cells were maintained with medium replenishment every 3 days. MSCs were then induced with mineralized medium (10 mM of β-glycerophosphate and 200 μM of L-ascorbic acid). After 12 days, cells were fixed with 4% paraformaldehyde and washed with PBS twice, and then stained with Alizarin Red S for 3 min.

4.12. Western blotting assay

Cell lysates were boiled in SDS sample buffer. Samples were electrophoresed on 10% SDS-PAGE gels and then transferred to polyvinylidene difluoride membranes (Millipore). The membranes were blocked with 5% skimmed milk in TBST buffer (50 mM Tris-HCl [pH7.4], 150 mM NaCl, and 0.1% Tween 20) for 1 h, then incubated with primary antibodies overnight at 4 °C and secondary antibodies for 1 h at room temperature. Proteins were detected using the ECL system (Thermo).

4.13. Quantitative Real-Time PCR analysis

Total RNA was isolated from 3T3-L1 adipocytes using TRIzol reagent and 3 μg of RNA was reverse transcribed to cDNA. Quantitative PCR analysis was performed using FastStart Universal SYBR Green Master. The relative amount of mRNA was calculated and normalized to GAPDH. The sequences of the primers were as follows: aP2-F: 5′-AAGGTGAAGAGCATCATAACCCT-3′; aP2-R: 5′- TCACGCCTTTCATAACACATTCC -3′; PPARγ-F: 5′- GCATGGTGCCTTCGCTGA-3′; PPARγ-R: 5′- TGGCATCTCTGTGTCAACCATG-3′; GAPDH-F: 5′- TGCACCACCAACTGCTTAGC-3′; GAPDH-R: 5′- GGATGCAGGGATGATGTTCT -3′.

4.14. Alkaline phosphatase activity assay

Cells were lysed in lysis buffer (150 mM NaCl, 1% NP-40, 50 mM Tris [pH 8.0]). Lysates were mixed with chromogenic substrate for 10 min. ALP activity was detected by Promega Microplate Reader, and the values were normalized to protein concentrations measured by Pierce BCA Protein Assay Kit.

4.15. In vitro cyclooxygenase (COX) inhibition assay

The probe is catalyzed by COX-2 to the fluorescence substance (ex560/em590). There is linear correlation between the COX-2 activity and the fluorescence intensity. In brief, COX-2 cofactor, COX-2 protein and compounds or DMSO were added to the COX-2 assay buffer for incubation at 37 °C for 10 min. The probe was added to the reaction buffer and mixed well. Arachidonic acid was then added to the reaction buffer and the fluorescence intensity was measured at the Tecan Spark Microplate Reader.

4.16. Stability of ***6b*** in rat liver microsome

6b in DMSO (4 μL, 0.4 mM) was added to 396 μL microsome suspension. The resulting mixture was incubated at 37 °C, and the catalytic reactions were then quenched at 0 min, 5 min 15 min, 30 min, 45 min, or 90 min by adding 1,200 μL of cold MeOH. The mixture was centrifuged at 13,000 rpm for 10 min and the supernatants were transferred to a glass tube and dried over nitrogen. The dried residue was reconstituted with 70% MeOH and analyzed with Thermo Fisher Scientific Q Exactive Orbitrap Mass Spectrometers (LC-MS). Microsome suspension: 364 μL phosphate buffer (Corning, 451201) + 8 μL rat liver microsome (Corning, 452511) + 4 μL solution A (Corning, 451220) + 4 μL solution B (Corning, 451200).

4.17. In vivo pharmacokinetic study of ***6b***

All animal experiments were approved by the Animal Care and Use Committee of Xiamen University, in accordance with the animal care and use guidelines. **6b** was dissolved in phosphate-buffered saline (pH 7.4) containing 5% (w/v) Solutol HS 15 (Sigma, 70142-34-6). **6b** solution was administered orally at the dosage of 30 mg/kg or intravenously at the dosage of 3 mg/kg to Sprague-Dawley (SD) Rats (180−220 g) after overnight fasting. Blood samples (400 μL) were collected at 0, 0.25, 0.5, 1, 2, 3, 4, 6, 8, 10 and 12 h after administration of **6b**. The blood samples were centrifuged to obtain plasma at 4 °C and at 4,000 g. These plasma samples (100 μL) were used for the quantification of **6b** concentration by Thermo Fisher Scientific Ultimate 3000HPLC and Orbitrap.

4.18. Statistical analysis

The data are presented as mean ± SD or mean ± SEM and represent at least two independent experiments. Two-tailed unpaired Student's *t*-test or Two-way ANOVA were used for statistical analysis using the GraphPad Prism 5.0 software. For all statistical analysis: *$p < 0.05$, **$p < 0.01$, ***$p < 0.001$, ****$p < 0.0001$ and ns $p > 0.05$.

Author contributions

Organic synthesis, W.Z., Z.Y., L.Y.; NMR and HPLC measurement and spectra interpretation, Z.Z., W.Z., Z.Y., Q.Y., H.Y.; molecular docking and structural comparison, Z.Z; fluorescence titration assay, F.H., J-j.C.; in vitro and in vivo evaluation of biological activities, F.H., Y.L.; metabolic stability and pharmacokinetic study, J-y.C., C.W.; original draft preparation, F.H., Z.Z., X.Z., Y.S., H.Z.; supervision, Y.S., H.Z.. All authors have given approval to the final version of the manuscript.

Declaration of competing interest

The authors declare that they have no known competing financial interests or personal relationships that could have appeared to influence the work reported in this paper.

Acknowledgements

This work was supported in part by National Natural Science Foundation of China (31770811 and 32070779); the Fundamental Research Funds for the Central Universities (20720200009 and 20720180052); Regional Demonstration of Marine Economy Innovative Development Project (14PYY051SF04 and 12PYY001SF08); the Natural Science Foundation of Fujian Province of China (2018J01133); and Youth Innovation Fund from Xiamen City (3502Z20206033).

Abbreviations used

DM	Dimethyl sulfoxide
DMSO	Dimethyl sulfoxide
RGZ	Rosiglitazone
RLA	relative luciferase activity
WY	wy14643
GW	gw501516
Alp	Alkaline phosphatase
HFD	High fat diet
PA	palmitic acid
IBMX	3-Isobutyl-1-methylxanthine
RNA	Ribo nucleic Acid
mRNA	messenger RNA
RLE	relative expression
aP2	Adipocyte Protein 2
PPARγ	peroxisome proliferators-activated receptor gamma
PPARα	peroxisome proliferators-activated receptor alpha
PPARβ	peroxisome proliferators-activated receptor beta
RXRα	Retinoid X receptor alpha
PPRE	peroxisome proliferator response element

Luc	Luciferase
TA	transcriptional activity
Max	Maximum
p-AKT	Phospho-Akt/protein kinase B
PH	Hydrogen ion concentration
μM	Micromoles per liter
mM	Millimoles per liter

Appendix A. Supplementary data

Supplementary data to this article can be found online at https://doi.org/10.1016/j.ejmech.2021.113542.

References

[1] W.D. Rees, C.J. McNeil, C.A. Maloney, The Roles of PPARs in the Fetal Origins of Metabolic Health and Disease, vol. 2008, PPAR research, 2008, p. 459030.
[2] R.K. Semple, V.K. Chatterjee, S. O'Rahilly, PPAR gamma and human metabolic disease, J. Clin. Invest. 116 (2006) 581–589.
[3] T.M. Willson, M.H. Lambert, S.A. Kliewer, Peroxisome proliferator-activated receptor gamma and metabolic disease, Annu. Rev. Biochem. 70 (2001) 341–367.
[4] B.M. Forman, P. Tontonoz, J. Chen, R.P. Brun, B.M. Spiegelman, R.M. Evans, 15-Deoxy-Delta(12,14)-Prostaglandin J(2) is a ligand for the adipocyte determination factor Ppar-gamma, Cell 83 (1995) 803–812.
[5] J.T. Huang, J.S. Welch, M. Ricote, C.J. Binder, T.M. Willson, C. Kelly, J.L. Witztum, C.D. Funk, D. Conrad, C.K. Glass, Interleukin-4-dependent production of PPAR-gamma ligands in macrophages by 12/15-lipoxygenase, Nature 400 (1999) 378–382.
[6] S.A. Kliewer, J.M. Lenhard, T.M. Willson, I. Patel, D.C. Morris, J.M. Lehmann, A prostaglandin J(2) metabolite binds peroxisome proliferator-activated receptor-gamma and promotes adipocyte differentiation, Cell 83 (1995) 813–819.
[7] L. Nagy, P. Tontonoz, J.G.A. Alvarez, H.W. Chen, R.M. Evans, Oxidized LDL regulates macrophage gene expression through ligand activation of PPAR gamma, Cell 93 (1998) 229–240.
[8] K. Yu, W. Bayona, C.B. Kallen, H.P. Harding, C.P. Ravera, G. Mcmahon, M. Brown, M.A. Lazar, Differential activation of peroxisome proliferator-activated receptors by eicosanoids, J. Biol. Chem. 270 (1995) 23975–23983.
[9] H.E. Xu, M.H. Lambert, V.G. Montana, K.D. Plunket, L.B. Moore, J.L. Collins, J.A. Oplinger, S.A. Kliewer, R.T. Gampe Jr., D.D. McKee, J.T. Moore, T.M. Willson, Structural determinants of ligand binding selectivity between the peroxisome proliferator-activated receptors, Proc. Natl. Acad. Sci. U.S.A. 98 (2001) 13919–13924.
[10] J.M. Lehmann, L.B. Moore, T.A. Smith-Oliver, W.O. Wilkison, T.M. Willson, S.A. Kliewer, An antidiabetic thiazolidinedione is a high affinity ligand for peroxisome proliferator-activated receptor gamma (PPAR gamma), J. Biol. Chem. 270 (1995) 12953–12956.
[11] R. Basu, P. Shah, A. Basu, B. Norby, B. Dicke, V. Chandramouli, O. Cohen, B.R. Landau, R.A. Rizza, Comparison of the effects of pioglitazone and metformin on hepatic and extra-hepatic insulin action in people with type 2 diabetes, Diabetes 57 (2008) 24–31.
[12] N. Saraf, P.K. Sharma, S.C. Mondal, V.K. Garg, A.K. Singh, Role of PPARg2 transcription factor in thiazolidinedione-induced insulin sensitization, J. Pharm. Pharmacol. 64 (2012) 161–171.
[13] S.E. Nissen, K. Wolski, Effect of rosiglitazone on the risk of myocardial infarction and death from cardiovascular causes, N. Engl. J. Med. 356 (2007) 2457–2471.
[14] P.D. Home, S.J. Pocock, H. Beck-Nielsen, P.S. Curtis, R. Gomis, M. Hanefeld, N.P. Jones, M. Komajda, J.J. McMurray, R.S. Team, Rosiglitazone evaluated for cardiovascular outcomes in oral agent combination therapy for type 2 diabetes (RECORD): a multicentre, randomised, open-label trial, Lancet 373 (2009) 2125–2135.
[15] M. Ahmadian, J.M. Suh, N. Hah, C. Liddle, A.R. Atkins, M. Downes, R.M. Evans, PPARgamma signaling and metabolism: the good, the bad and the future, Nat. Med. 19 (2013) 557–566.
[16] T.T. Ashburn, K.B. Thor, Drug repositioning: identifying and developing new uses for existing drugs, Nature reviews, Drug Discov. 3 (2004) 673–683.
[17] D.C. Swinney, J. Anthony, How were new medicines discovered? Nat. Rev. Drug Discov. 10 (2011) 507–519.
[18] T.L. Doan, M. Pollastri, M.A. Walters, G.I. Georg, The Future of Drug Repositioning 46, 2011, pp. 385–401.
[19] A.C. Puhl, F.A. Milton, A. Cvoro, D.H. Sieglaff, J.C. Campos, A. Bernardes, C.S. Filgueira, J.L. Lindemann, T. Deng, F.A. Neves, I. Polikarpov, P. Webb, Mechanisms of peroxisome proliferator activated receptor gamma regulation by non-steroidal anti-inflammatory drugs, Nucl. Recept. Signal. 13 (2015), e004.
[20] M. Wick, G. Hurteau, C. Dessev, D. Chan, M.W. Geraci, R.A. Winn, L.E. Heasley, R.A. Nemenoff, Peroxisome proliferator-activated receptor-gamma is a target of nonsteroidal anti-inflammatory drugs mediating cyclooxygenase-independent inhibition of lung cancer cell growth, Mol. Pharmacol. 62 (2002) 1207–1214.
[21] M. Sastre, I. Dewachter, S. Rossner, N. Bogdanovic, E. Rosen, P. Borghgraef, B.O. Evert, L. Dumitrescu-Ozimek, D.R. Thal, G. Landreth, J. Walter, T. Klockgether, F. van Leuven, M.T. Heneka, Nonsteroidal anti-inflammatory drugs repress beta-secretase gene promoter activity by the activation of PPARgamma, Proc. Natl. Acad. Sci. U.S.A. 103 (2006) 443–448.
[22] A. Munjal, R. Wadhwa, Sulindac, in: StatPearls, Treasure Island (FL), 2020.
[23] H. Zhou, W. Liu, Y. Su, Z. Wei, J. Liu, S.K. Kolluri, H. Wu, Y. Cao, J. Chen, Y. Wu, T. Yan, X. Cao, W. Gao, A. Molotkov, F. Jiang, W.G. Li, B. Lin, H.P. Zhang, J. Yu, S.P. Luo, J.Z. Zeng, G. Duester, P.Q. Huang, X.K. Zhang, NSAID sulindac and its analog bind RXRalpha and inhibit RXRalpha-dependent AKT signaling, Canc. Cell 17 (2010) 560–573.
[24] S. Grosch, T.J. Maier, S. Schiffmann, G. Geisslinger, Cyclooxygenase-2 (COX-2)-independent anticarcinogenic effects of selective COX-2 inhibitors, J. Natl. Cancer Inst. 98 (2006) 736–747.
[25] A.S. Felts, B.S. Siegel, S.M. Young, C.W. Moth, T.P. Lybrand, A.J. Dannenberg, L.J. Marnett, K. Subbaramaiah, Sulindac derivatives that activate the peroxisome proliferator-activated receptor gamma but lack cyclooxygenase inhibition, J. Med. Chem. 51 (2008) 4911–4919.
[26] A.C. Puhl, F.A. Milton, A. Cvoro, D.H. Sieglaff, J.C.L. Campos, A. Bernardes, C.S. Filgueira, J.L. Lindemann, T. Deng, F.A.R. Neves, I. Polikarpov, P. Webb, Mechanisms of peroxisome proliferator activated receptor gamma regulation by non-steroidal anti-inflammatory drugs, Nucl. Recept. Signal. 13 (2015) e004-e004.
[27] Z.G. Wang, L.Q. Chen, J.B. Chen, J.F. Zheng, W.W. Gao, Z.P. Zeng, H. Zhou, X.K. Zhang, P.Q. Huang, Y. Su, Synthesis and SAR study of modulators inhibiting tRXR alpha-dependent AKT activation, Eur. J. Med. Chem. 62 (2013) 632–648.
[28] Z.Q. Yan, S.Y. Chong, H.Y. Lin, Q. Yang, X. Wang, W.D. Zhang, X.K. Zhang, Z.P. Zeng, Y. Su, Design, synthesis and biological evaluation of tetrazole-containing RXR alpha ligands as anticancer agents, Eur. J. Med. Chem. 164 (2019) 562–575.
[29] P. Tontonoz, E. Hu, R.A. Graves, A.I. Budavari, B.M. Spiegelman, mPPAR gamma 2: tissue-specific regulator of an adipocyte enhancer, Gene Dev. 8 (1994) 1224–1234.
[30] P. Tontonoz, B.M. Spiegelman, Fat and beyond: the diverse biology of PPARgamma, Annu. Rev. Biochem. 77 (2008) 289–312.
[31] B.M. Spiegelman, L. Choy, G.S. Hotamisligil, R.A. Graves, P. Tontonoz, Regulation of adipocyte gene expression in differentiation and syndromes of obesity/diabetes, J. Biol. Chem. 268 (1993) 6823–6826.
[32] E. Calvo-Ochoa, K. Sanchez-Alegria, C. Gomez-Inclan, P. Ferrera, C. Arias, Palmitic acid stimulates energy metabolism and inhibits insulin/PI3K/AKT signaling in differentiated human neuroblastoma cells: the role of mTOR activation and mitochondrial ROS production, Neurochem. Int. 110 (2017) 75–83.
[33] S.C. Benoit, C.J. Kemp, C.F. Elias, W. Abplanalp, J.P. Herman, S. Migrenne, A.L. Lefevre, C. Cruciani-Guglielmacci, C. Magnan, F. Yu, K. Niswender, B.G. Irani, W.L. Holland, D.J. Clegg, Palmitic acid mediates hypothalamic insulin resistance by altering PKC-theta subcellular localization in rodents, J. Clin. Invest. 119 (2009) 2577–2589.
[34] M. Van Beek, K.I. Oravecz-Wilson, P.C. Delekta, S. Gu, X. Li, X. Jin, I.J. Apel, K.S. Konkle, Y. Feng, D.H. Teitelbaum, J. Ruland, L.M. McAllister-Lucas, P.C. Lucas, Bcl10 links saturated fat overnutrition with hepatocellular NF-kB activation and insulin resistance, Cell Rep. 1 (2012) 444–452.
[35] A.V. Schwartz, D.E. Sellmeyer, E. Vittinghoff, L. Palermo, B. Lecka-Czernik, K.R. Feingold, E.S. Strotmeyer, H.E. Resnick, L. Carbone, B.A. Beamer, S.W. Park, N.E. Lane, T.B. Harris, S.R. Cummings, Thiazolidinedione use and bone loss in older diabetic adults, J. Clin. Endocrinol. Metabol. 91 (2006) 3349–3354.
[36] A. Grey, M. Bolland, G. Gamble, D. Wattie, A. Horne, J. Davidson, I.R. Reid, The peroxisome proliferator-activated receptor-gamma agonist rosiglitazone decreases bone formation and bone mineral density in healthy postmenopausal women: a randomized, controlled trial, J. Clin. Endocrinol. Metabol. 92 (2007) 1305–1310.
[37] S. Yaturu, B. Bryant, S.K. Jain, Thiazolidinedione treatment decreases bone mineral density in type 2 diabetic men, Diabetes Care 30 (2007) 1574–1576.
[38] C. Wang, Y. Wang, N.T. Huffman, C. Cui, X. Yao, S. Midura, R.J. Midura, J.P. Gorski, Confocal laser Raman microspectroscopy of biomineralization foci in UMR 106 osteoblastic cultures reveals temporally synchronized protein changes preceding and accompanying mineral crystal deposition, J. Biol. Chem. 284 (2009) 7100–7113.
[39] A.A. Ali, R.S. Weinstein, S.A. Stewart, A.M. Parfitt, S.C. Manolagas, R.L. Jilka, Rosiglitazone causes bone loss in mice by suppressing osteoblast differentiation and bone formation, Endocrinology 146 (2005) 1226–1235.
[40] C. Liu, T. Feng, N. Zhu, P. Liu, X. Han, M. Chen, X. Wang, N. Li, Y. Li, Y. Xu, S. Si, Identification of a novel selective agonist of PPARgamma with no promotion of adipogenesis and less inhibition of osteoblastogenesis, Sci. Rep. 5 (2015) 9530.
[41] F. Zhang, B.E. Lavan, F.M. Gregoire, Selective Modulators of PPAR-Gamma Activity: Molecular Aspects Related to Obesity and Side-Effects, vol. 2007, PPAR research, 2007, p. 32696.
[42] T. Akune, S. Ohba, S. Kamekura, M. Yamaguchi, U.I. Chung, N. Kubota, Y. Terauchi, Y. Harada, Y. Azuma, K. Nakamura, T. Kadowaki, H. Kawaguchi, PPARgamma insufficiency enhances osteogenesis through osteoblast formation from bone marrow progenitors, J. Clin. Invest. 113 (2004) 846–855.

[43] J.Y. Jang, H. Bae, Y.J. Lee, Y.I. Choi, H.J. Kim, S.B. Park, S.W. Suh, S.W. Kim, B.W. Han, Structural basis for the enhanced anti-diabetic efficacy of lobeglitazone on PPARgamma, Sci. Rep. 8 (2018) 31.
[44] Z.X. Wang, N.R. Kumar, D.K. Srivastava, A novel spectroscopic titration method for determining the dissociation constant and stoichiometry of protein-ligand complex, Anal. Biochem. 206 (1992) 376–381.
[45] K. Zebisch, V. Voigt, M. Wabitsch, M. Brandsch, Protocol for effective differentiation of 3T3-L1 cells to adipocytes, Anal. Biochem. 425 (2012) 88–90.
[46] A. Mehlem, C.E. Hagberg, L. Muhl, U. Eriksson, A. Falkevall, Imaging of neutral lipids by oil red O for analyzing the metabolic status in health and disease, Nat. Protoc. 8 (2013) 1149–1154.